UNIVERSITY OF OKLAHOMA

GRADUATE COLLEGE

MANUFACTURING OF CONTINUOUS CARBON FIBER COMPOSITES USING ULTRAVIOLET LASER-ASSISTED DIRECT INK WRITE 3D PRINTING

A THESIS

SUBMITTED TO THE GRADUATE FACULTY

in partial fulfillment of the requirements for

Degree of

MASTER OF SCIENCE

By

RYAN COWDREY
Norman, Oklahoma
2020

MANUFACTURING OF CONTINUOUS CARBON FIBER COMPOSITES USING

ULTRAVIOLET LASER-ASSISTED DIRECT INK WRITE 3D PRINTING

A THESIS APPROVED FOR THE
SCHOOL OF AEROSPACE AND MECHANICAL ENGINEERING

BY THE COMMITTEE CONSISTING OF

Dr. Yingtao Liu, Chair

Dr. Mrinal C. Saha, Co-Chair

Dr. M. Cengiz Altan

Acknowledgements

I would like to first thank Dr. Yingtao Liu at the University of Oklahoma (OU) for allowing me the opportunity to work in his research group over the past two years. Through his mentorship, I have grown as a researcher and engineer and have learned a lot from him. I am especially grateful for the freedom he gave me to explore new ideas that interested me and to change the scope of my research accordingly. He encouraged me to read published literature and think beyond what has already been done, and it was this support that allowed me to develop this innovative project. I would also like to thank Dr. Mrinal Saha as well for his support over the past two years. His input was also helpful in the development of my project, and I appreciate him taking the time each week to meet with our lab group to better our research as a whole. I would also like to thank Dr. Cengiz Altan for taking the time to participate as a member of my defense committee. My short time in graduate school has been fairly unconventional, starting with a shoulder injury requiring surgery and several months of rehabilitation, and ending with two months of quarantine from all campus activities due to the COVID-19 outbreak. Through this all I am appreciative of the efforts of the faculty and staff of the School of Aerospace and Mechanical Engineering (AME) to remain flexible and assist students throughout these hardships.

I have really enjoyed my time in research at OU due in large part to the people I have worked with. I would especially like to thank the members of our research lab, Blake Herren, Colin Bray, Weston Sleeper, Ben Hoelzel, and Noah Golly for making our lab an enjoyable place to come work every day. I appreciate the assistance they provided with my project and am especially grateful for the friendships we formed in this time. I would also like to thank Antonio Santiago and the members of the AME machine shop for their assistance machining parts for me.

I’d also like to thank all of the friends I have made as a member of the Sooner Racing Team over the past five years I was on the team. Starting out on the team as a freshman I learned so much from the older members, and I was very grateful to get the opportunity to lead the team as an upperclassman. These experiences of learning engineering design, manufacturing, leadership, and teamwork shaped who I am as an engineer today. I’d like to especially thank Dr. Zahed Siddique for his guidance as advisor to the team, Billy Mays, Greg Williams, and Jimmy Cannon for their support in the machine shops, and the entire AME office staff including Bethany Burklund, Martina Ferguson, Melissa Foster, Ellen McKenzie, and Rebeka Morales who have helped me out in numerous ways over the past several years.

Finally, I would like to thank my family and friends who have supported me throughout my life. I am very grateful for my parents and older brother, who have always been supportive and loving to me, and have always encouraged me to follow my dreams. I am also grateful for all my friends from high school and college, who always make life fun and entertaining. It is these family members and friends that have shaped who I am today, and I am very thankful for all that they do for me.

Table of Contents

Table of Figures

Table of Tables

Abstract

Additive manufacturing (AM), commonly referred to as 3D printing, is a quickly growing field with numerous techniques available to manufacture parts which are stronger, lighter, and more complex than those which could be traditionally manufactured. With the goal of creating stronger parts, a new 3D printing technique was developed which combined properties of several different methods in order to print continuous carbon fiber-reinforced thermosets. This new method is called continuous fiber direct writing (CFDW). The process works by extruding continuous fiber and ultraviolet (UV) curable resin out of a syringe simultaneously and curing the resin immediately upon extrusion via UV lasers aimed at the extrusion point. This was created using the principles behind direct ink writing (DIW), stereolithography (SLA), and fused deposition modeling (FDM). It utilizes DIW technology to extrude liquid resin out of the syringe, SLA technology to cure the resin in situ, and FDM technology to deposit the fiber and resin onto the print path. In order to test this novel method, a custom extrusion system and print head was designed and adapted onto an existing consumer FDM printer. The developed printer is able to successfully print continuous fiber-reinforced samples with control over the fiber direction and fiber volume fraction. Several experiments were conducted in order to characterize the various printing parameters. The largest focus was on the two most important parameters: deposition speed and extrusion pressure. The deposition speed, or feed rate, describes how quickly the print head moves across the build plate, while the extrusion pressure describes how much pressure is applied to extrude the resin out of the syringe. These two parameters together greatly affect the resulting width and shape of a printed line of fiber. In general, increasing the pressure or decreasing the feed rate creates a larger line width. This is very important as it affects the hatch spacing which in turn affects the fiber volume fraction. Additionally, these factors can affect the top surface finish of the resulting part. In

addition to these parameter-based studies, bulk rectangular samples and complex samples were printed in order to demonstrate the capabilities of the printer. The CFDW method works well and is fairly consistent with the proper printing parameters. Through future development of this process, composite samples can be made with individual tows of fibers oriented according to the geometry of the part, allowing for reduced weight and increased strength of the additively manufactured components.

CHAPTER 1: INTRODUCTION

1.1: Additive Manufacturing Processes for Polymer Materials

The field of additive manufacturing describes a wide variety of manufacturing methods used to manufacture polymers, metals, ceramics, composites, and biomaterials [1-4]. There are several different methods of AM which are used to create parts layer-by-layer. One method may be chosen over another due to its suitability for a certain material, advantages in precision, print speed, or cost-effectiveness [5]. The most common methods of AM are shown in Table 1.

Table 1: Overview of common AM processes [6]

Method	Similar Processes	Materials
Binder jetting	Ink-jetting	Metal powders Polymer powders Ceramic powders
Direct energy deposition	Direct metal deposition	Metal powders Metal wires
Direct ink writing	Bioprinting Robocasting	Biomaterial inks Polymer inks
Fused deposition modeling	Fused filament fabrication	Polymer filaments
Material jetting	Inkjet printing	Photopolymer inks
Selective laser sintering	Selective laser melting Electron beam melting Powder bed fusion	Metal powders Polymer powders Ceramic powders
Sheet lamination	Ultrasonic additive manufacturing	Hybrid sheets Metal sheets Ceramic sheets
Vat photopolymerization	Stereolithography Digital light processing Continuous liquid interface production	Photopolymer resins

As polymer additive manufacturing continues to evolve, new methods are being developed to increase the strength of printed parts. One method to do this is to use reinforcing fibers in the polymer. Using continuous fibers to reinforce 3D prints makes them much stronger and stiffer, leading to their potential use in many engineering applications. Several new techniques for manufacturing continuous fiber-reinforced polymers have been developed and are based upon the principles of fused deposition modeling, stereolithography, directed energy deposition (DED), and direct ink writing [7-14]. These forms of additive manufacturing are described in greater detail in the following sections.

1.2: Fused Deposition Modeling

One of the most widely used methods of AM is fused deposition modeling. First patented in 1989 by S. Scott and Lisa Crump, this process has become widespread in both the consumer and industrial markets [15]. The patents for FDM expired in 2005, allowing many new manufacturers to start producing these printers, many of whom open-sourced their technology [15]. FDM works by heating a thermoplastic to a viscous state and extruding it out of the nozzle of the print head [16]. In doing so, the printer builds up a part layer-by-layer until it is complete. Recently, several manufacturers have released novel FDM 3D printers for the additive manufacturing of multi-materials using multi-nozzle printing system. Due to the high spatial resolution, these printers can achieve high surface smoothness and overall quality. Figure 1 shows a diagram of an FDM printer with two nozzles: one to extrude print material and the other to extrude support material. This is common in high end printers, as it allows for the support material to be easily dissolved in a solvent to remove it after the print is completed.

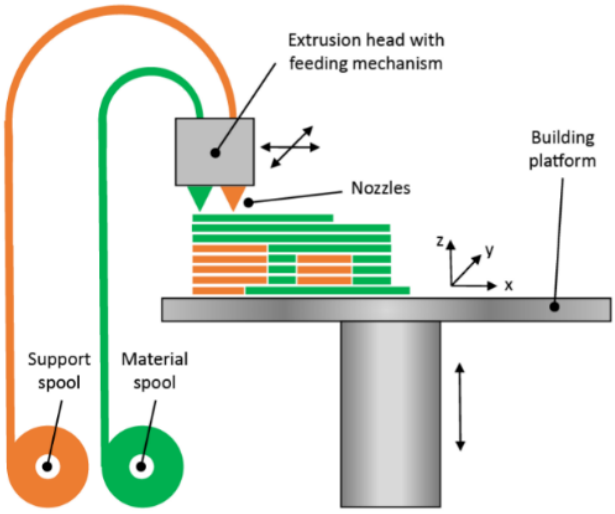

Figure 1: Illustration of FDM process [17]

The plastic is usually kept on a spool in the form of filament approximately 1.75 mm in diameter. Some printers, however, take in pellets or powder and melt it down as needed. There are a wide variety of filaments available, with the most common being polylactide acid (PLA), which is regarded as the easiest material to print with, and acrylonitrile butadiene styrene (ABS) which is much tougher but is more difficult to print due to its higher melting temperature [18]. The printers themselves have heated nozzles to heat the filament, and heated beds to improve bed adhesion by significantly reducing thermal gradients. FDM is great for prototyping and is very cost effective and simple to use.

The downsides to FDM are the thermoplastics the method is limited to printing. Printed thermoplastics parts cannot perform in high-temperature environments and are generally low strength and are moderately anisotropic. Additionally, it can be difficult to print large parts as internal stresses generated in the part as material cools and shrinks coming out of the nozzle can warp the part and pull it off of the build plate [19]. Post-processing for FDM includes removing

support materials if used, and sanding or vapor smoothing (using a vaporized solvent to slightly dissolve the surface layer) to improve the surface finish.

1.3: Stereolithography

SLA is another commonly used AM method. This method became the first patented 3D printing method when Charles Hull patented it in 1986 [20]. SLA uses a pool of liquid photopolymer and an ultraviolet laser to cure the material. In SLA, the laser scans the pattern of a single slice, the bed lowers to allow fresh liquid to flow on top of the print, and the laser scans the next slice until the part is complete [21]. Figure 2 shows two common methods of SLA. The left illustration shows the laser curing material from the top and the platform lowering in the bath, while the right illustration shows the platform raising up out of the bath with the laser curing the material from the bottom.

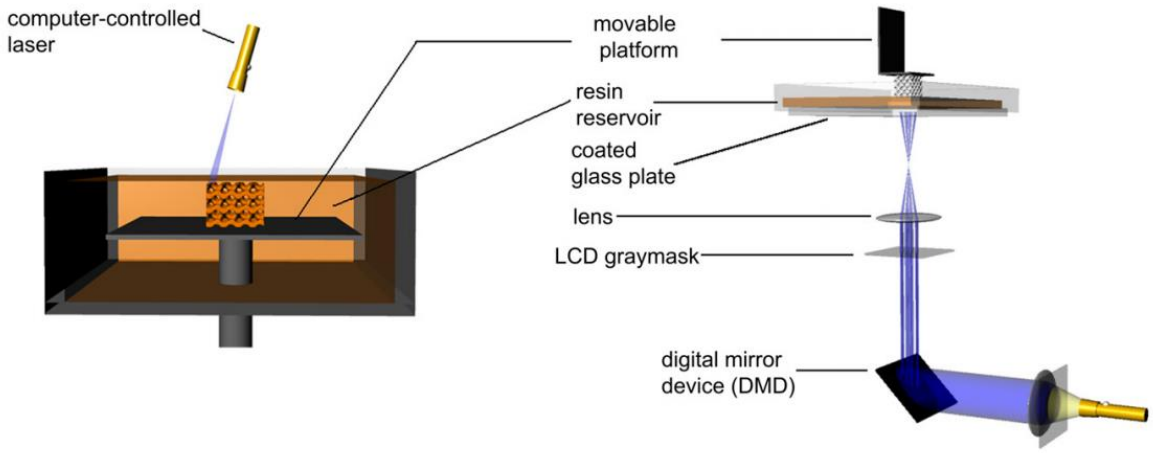

Figure 2: Illustration of SLA process [22]

SLA is a subset of the vat polymerization category, which includes similar methods such as digital light processing (DLP) and continuous liquid interface production (CLIP). DLP and CLIP utilize a projector sitting under a photopolymer bath as a light source which can cure an entire slice simultaneously, instead of having a laser trace out the image [23]. SLA prints with photopolymer

materials, which are formulated specifically for SLA printers. Like FDM, these prints also suffer from issues of bed adhesion and warping, as the material shrinks when it is cured [24]. Some of the benefits of SLA are that it prints thermosets, the resolution can be very fine since it is cured with the laser, and the parts can be made transparent or translucent, which is not done in any other form of 3D printing. Post-processing for these prints involves post-curing the print under ultraviolet lights to ensure it is fully cured.

1.4: Directed Energy Deposition

DED is a process in which metal or polymer is fed in the form of wire or powder and is melted with lasers to deposit liquid material on the part [25]. The laser and the material meet at the same point to melt the material, which quickly solidifies as it cools. An illustration of this process is shown in Figure 3.

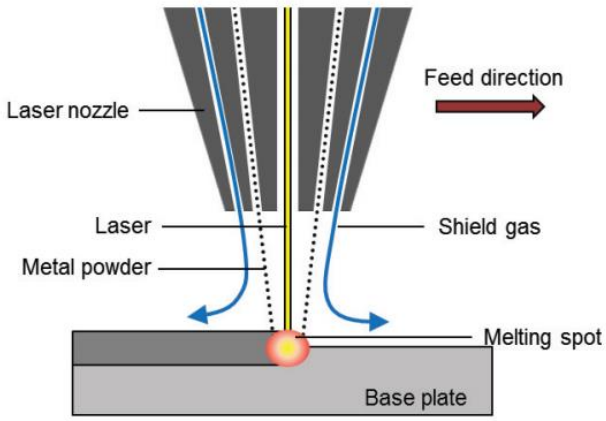

Figure 3: Illustration of DED process [26]

This process is less precise than other methods, and results in a near-net finished part which requires machining to improve the surface finish [25]. DED is one of the two main methods for metal AM parts. Metal parts are more often manufactured by selective laser sintering (SLS), which uses a laser to sinter a bed of fine powder to melt particles together until it can be post-cured to

achieve full strength [27]. The benefit of DED is that it is much quicker than laser sintering, and it is able to produce much larger parts without wasting excess powder in a bed. DED is not widely used for polymers due to the much better methods of FDM or SLA to create those parts, but it does share similarities with the CFDW process.

1.5: Direct Ink Writing

Direct ink writing, sometimes referred to as robocasting or bioprinting, is a method in which viscous inks are printed onto a substrate. This is done by loading material into a syringe and using pneumatics, hydraulics, or mechanical displacement to force the material out of the syringe in a controlled manner [28]. Materials in this method are very wide ranging, as anything with a high enough viscosity can be printed, such as nanocomposite inks, photopolymers, biomaterials, ceramic slurries, and more [8, 29-32]. Figure 4 shows this process creating 2D lines and 3D lattice structures.

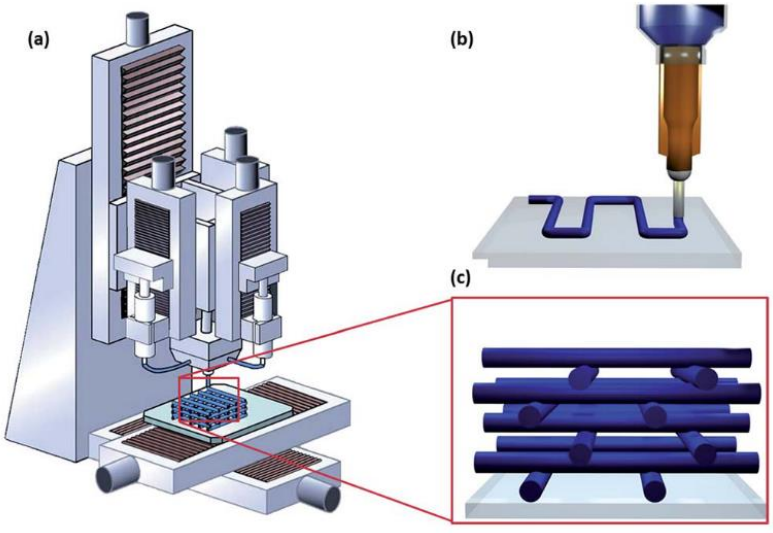

Figure 4: Illustration of DIW process [33]

The method for curing is dependent on the material. For a material which cures via heat, often a full print is completed and the entire sample is then cured in an oven [34, 35]. The material is still

able to be printed in this way since it has high enough yield strength so as not to deform excessively after it is deposited from the nozzle [36]. DIW can also be achieved with UV curing to solidify the material in situ as it comes out of the nozzle. The benefits of this 3D printing method are that it can use a very small amount of material if needed and can print almost any viscous liquid or gel. This method can also be used to embed a print inside a material bath. An illustration of this novel manufacturing process is shown in Figure 5. This figure shows embedded printing of a nanocomposite ink inside an elastic material to create highly stretchable strain sensors.

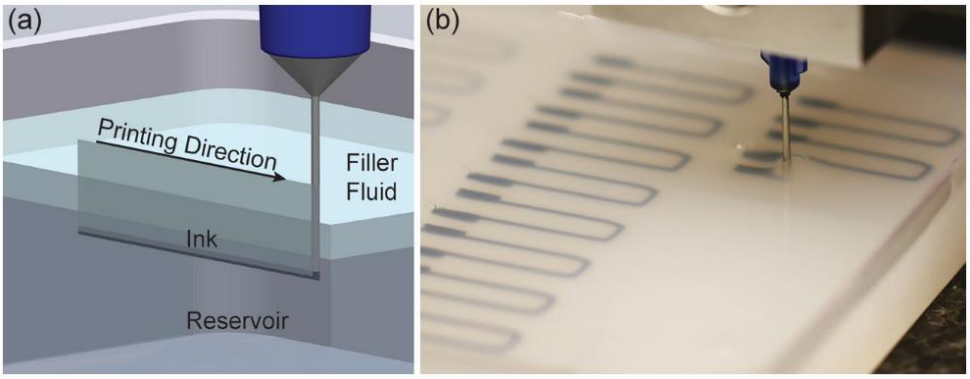

Figure 5: Embedded DIW printing

Embedded sensors are a growing field which rely on the use of DIW to print one material within another [37]. The downside of DIW is that there is not a way to cure in situ, meaning it may be difficult to print large or complicated geometries. Other material processing technologies, such as microwave curing, can also be integrated with the DIW 3D printing for the rapid manufacturing of nanocomposites [38-40].

1.6: Continuous Fiber-Reinforced 3D Printing

In order to 3D print continuous fiber-reinforced parts, there are currently two main printing techniques. The first is to reinforce FDM prints with fibers by feeding a tow of fiber through the

melted polymer in the print head and out the extrusion nozzle with the melted polymer [41]. An illustration of this process is shown in Figure 6.

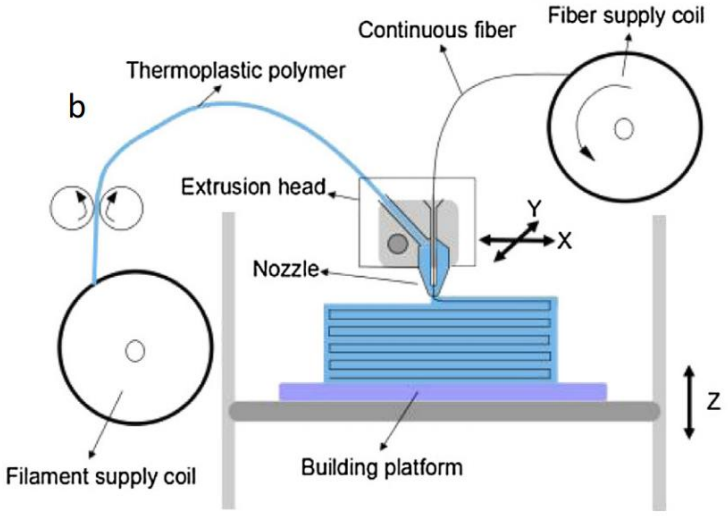

Figure 6: Illustration of continuous fiber FDM process [42]

These prints use the same materials found in typical FDM printing, mainly PLA and ABS. These parts are stronger than normal FDM parts, but still have the downsides associated with using thermoplastic matrices, such as lower strength and poor performance at elevated temperatures compared to thermosets. A similar technique was developed in which continuous fiber was coated in a viscous epoxy and fed through a printer as a filament [43]. As the filament reached the extruder, it was heated to decrease its viscosity so it could be printed, then was thermally post-cured to reach full strength [43]. This resulted in strong continuous fiber thermosetting 3D prints.

Another method is to use UV curing of a liquid resin on the fiber. The company Continuous Composites developed the method of continuous fiber 3D printing (CF3D) [44]. This company uses this method to create large composite structures out of carbon fiber, fiberglass, Kevlar, and more [44]. CF3D works by extruding dry fiber out of one nozzle and a photopolymer out of another. Right after the two materials meet, an ultraviolet light cures the polymer, giving it enough

yield strength to create freestanding structures. Using this process on large robotic arms has given the ability to create large high-performance composite structures without the use of molds or autoclaves, and with fewer geometric constraints [45]. One major benefit of this method is that it allows for the control of the fiber directions throughout the parts, meaning that some areas can be reinforced more if needed. Additionally, since the parts are created directly from the printer it is quicker than traditional composite manufacturing and does so with less material waste [44].

1.7: Polymer AM Materials

Polymer additive manufacturing includes a wide variety of materials including both thermoplastics and thermosets. The primary difference between these two categories is that thermoplastics can be melted and reshaped multiple times to form parts, while thermosets cannot be reshaped once they are formed [46]. This makes thermoplastics ideal for applications in which strength and temperature resistance are not of high importance, as they are generally cheap and easy to process. The two main thermoplastic printing methods are FDM, which melts and extrudes a filament, and SLS, which melts fine powder to fuse particles together. For applications in which higher strength or temperature resistance is needed, thermosets are better suited. Vat photopolymerization methods use a bath of photopolymer thermoset which is cured by the path of a UV laser. DIW methods can use UV curing, but also can use thermally cured epoxies which are printed and then post-cured in an oven. These thermally cured epoxies reach the highest strength of polymer AM prints. For fiber-reinforced 3D prints, a few materials have been used including PLA, ABS, UV resin, and epoxy. A comparison of the material properties of these materials is shown in Table 2.

Table 2: Comparison of polymer material properties used in CF 3D printing

	Makerbot PLA [47]	Makerbot ABS [48]	CPS PR-48 UV Resin [49]	E-20 Epoxy [43, 50]
Tensile yield strength (MPa)	62	43	28	60-77
Tensile modulus (MPa)	3,600	2,400	1,400	N/A
Elongation at break	>4.4%	>5.6%	3%	3.5-5.2%

Reinforcing fibers used in polymer AM are typically short fibers mixed into the material before printing [51]. Short carbon fiber-reinforced PLA and ABS filament can be purchased and printed on a normal FDM printer. It is also simple to mix fibers into an epoxy for use in DIW printing. Carbon fiber, glass fiber, and Kevlar have also been used as continuous fibers in 3D prints, which results in stronger prints [52]. A comparison of the material properties of these continuous fibers is shown in Table 3. These properties are given for a specific material and will vary depending on the actual fibers chosen.

Table 3: Comparison of common reinforcing fibers

	Carbon Fiber [53]	Glass Fiber [54]	Kevlar Fiber [55]
Tensile strength (MPa)	4,650	3,450-3,790	3,000
Tensile modulus (GPa)	231	72.4	112
Elongation at break	1.8%	4.8%	2.4%
Density (g/cc)	1.78	2.54-2.60	1.44

As seen from the material properties of these fibers, there is a benefit to each one. Using carbon fiber will result in the highest strength and stiffness. Glass fiber will provide the highest elongation at break, as well as the lowest cost. Lastly, using Kevlar will give the lowest weight, while still having a high modulus. Kevlar is also known for its toughness, making it ideal for applications in which this is needed.

1.8: Thesis Outline

The purpose of this thesis is to affordably create and analyze continuous carbon fiber samples manufactured via desktop UV laser-assisted 3D printing. Chapter 2 describes the design and construction of a 3D printer capable of printing such samples, which involves modifying an existing FDM printer, creating a pneumatic extrusion system, a new print head, and a continuous fiber reservoir. Chapter 3 discusses the process of creating samples and the printing parameters which can be adjusted. Chapter 4 provides a description of the analyses performed on the printing process, which includes a study of the printing parameters and capabilities of the printer. Finally, Chapter 5 presents the conclusions and future work for this project.

CHAPTER 2: DESIGN OF CONTINUOUS FIBER DIRECT WRITE PRINTER

2.1: Introduction

In order to additively manufacture continuous fiber composites, an FDM printer was purchased and converted to work as a direct ink write printer. This printer was first altered with a new print head with UV lasers and a new extrusion system to become an ultraviolet laser-assisted direct ink write 3D printer. Once this was done, it was found that fiber could be extruded through the printer, and a fiber chamber was added to allow the printer to manufacture continuous fiber composite parts. This method is unique from existing methods and is best described as continuous fiber direct writing.

2.2: Printer Conversion

The 3D printer used in the construction of the CFDW printer was a Creality CR-10 Mini, shown in Figure 7. This was a widely popular consumer FDM printer which moved the extruder in the X-axis, moved a heated build plate in the Y-axis, and raised the extruder in the Z-axis. The extruder could travel up to 300 mm in the horizontal directions, and 220 mm in the vertical direction [56].

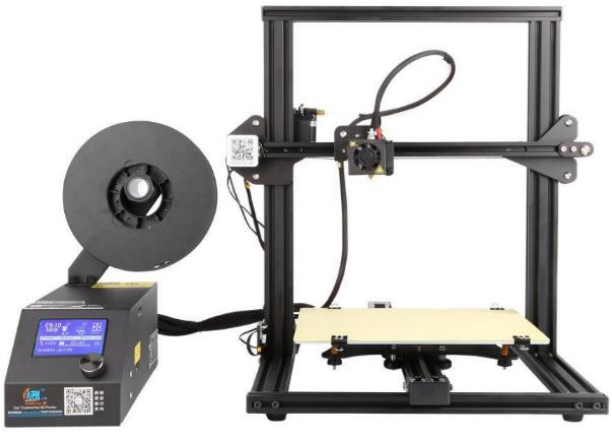

Figure 7: Creality CR-10 Mini as purchased [56]

This printer was chosen as the base due to its simple construction and rigid frame. It also provided a platform on which various modifications could be made. The printer was open source and had plenty of information available online regarding modifying the printer. The existing computer-aided design (CAD) 3D model was downloaded from the Creality open source files in order to design the new assembly [57]. The CAD model of the modified printer is shown in Figure 8. Due to the need for the printer controls to be accessed outside of an enclosure, the electronics were removed from the printer itself and moved outside of the enclosure. They are therefore not shown in the model.

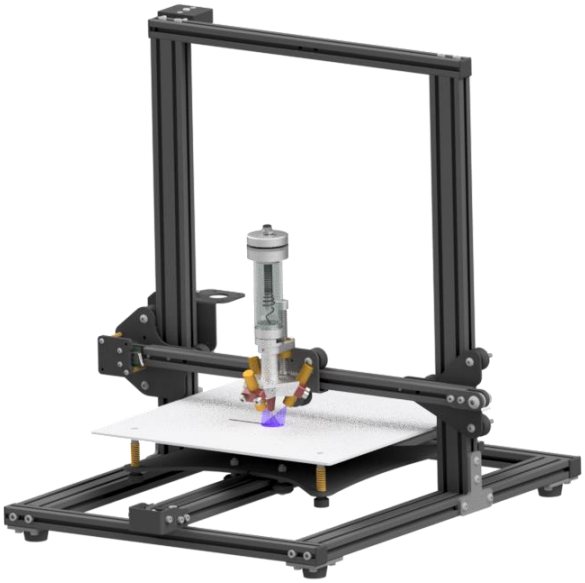

Figure 8: CAD model of CR-10 with modified print head assembly

Since UV light is dangerous to human eyes, the entire printer was operated inside of a metal enclosure with a small tinted window to view the prints. This enclosure was constructed using aluminum extruded bars attached together to build the frame, with sheet metal panels attached on the sides and top. The front panel was hinged like a door in order to access the printer. The completed printer in the enclosure is shown in Figure 9.

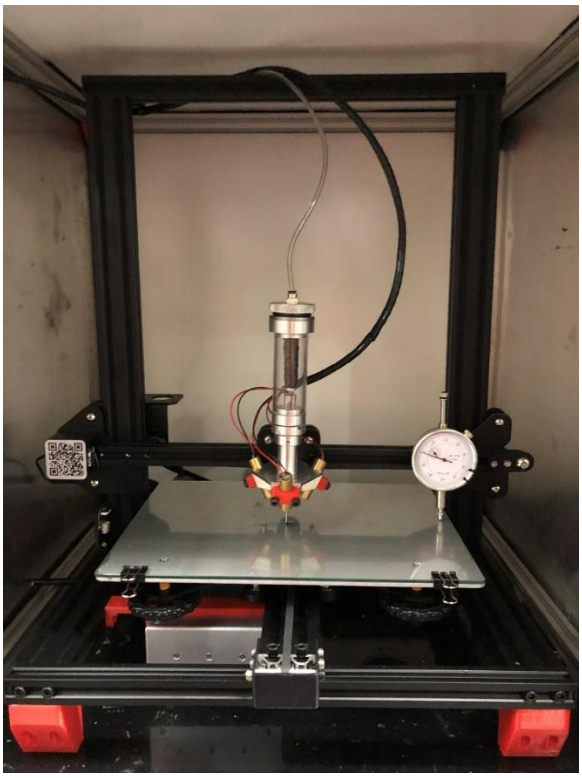

Figure 9: Image of completed printer inside enclosure

As seen in Figure 9, risers were added for the power supply to be mounted underneath the printer. A dial caliper was also added onto the Z-axis so that the distance from the extrusion nozzle to the plate could be consistently measured.

2.3: Pneumatic Extrusion System

In order to extrude liquid material out of a syringe, a pneumatic system was created and implemented on the printer. A pneumatic system was initially chosen over a mechanical plunger system due to issues seen on mechanically based extruders of pressure build-up during print moves, causing the material to continue to extrude during non-print moves. Using a pneumatic system solved this issue due to its ability to immediately apply and release pressure. This pressure system also allowed for the continuous fiber to be used, as it would not work with a mechanical plunger or screw since there would be no path for the fiber to travel. The system used on the CFDW

printer consisted of a pressure regulator, an electronic solenoid valve, and a syringe adapter. These components were mounted outside of the enclosure, so that they could be controlled and adjusted without opening the enclosure door. Pressurized air came into the printer (at about 600 kPa) via an air hose and flowed through a pressure regulator. This regulator, shown in Figure 10, regulated from 0-400 kPa, which was sufficient for extruding materials of much higher viscosities than were used in this study.

Figure 10: Image of pressure regulator mounted on wall outside of enclosure

This regulator allowed for the pressure seen at the syringe to be adjusted, which affected the rate of material flow out of the nozzle. From the regulator, the air flowed to a 12 volt (V) direct current (DC) normally closed electronic solenoid valve. The air from the solenoid valve output directly to the print head. Mounted with the solenoid was the voltage regulator used to control the power supplied to the lasers Additionally, a switch was mounted in order to turn off power to the laser from outside the printer to act as a kill switch, and to allow the printer to function as a direct ink write printer without the lasers turned on, should it be needed for other experiments. This electronics assembly is shown in Figure 11, and was also mounted to the wall outside the enclosure.

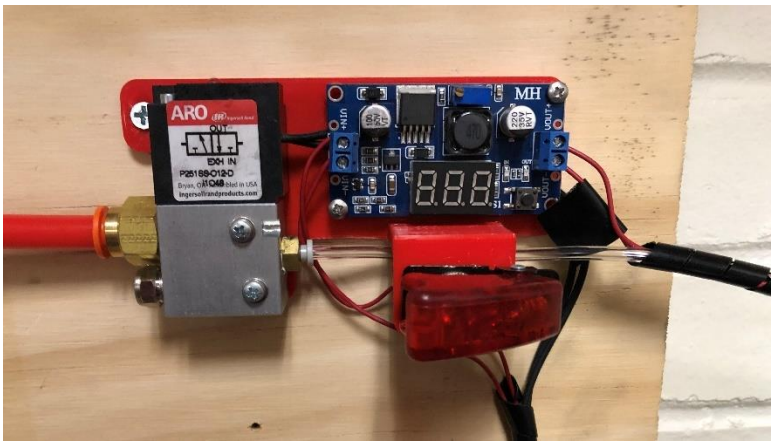

Figure 11: Image of pneumatic and laser electronics assembly

Both the solenoid valve and the lasers were wired to the motherboard, in parallel, using the "fan" output on the board. This allowed the printer to send current to the solenoid and lasers during the print using the g-code commands for "fan on" (M106 S255) and "fan off" (M107). The M106 S255 command opened the air valve and turned on the lasers, while M107 shut the valve and turned off the lasers. These commands could be used anywhere in the code to allow for starting and stopping prints, as well as doing non-print moves in which no material would be extruded or cured.

2.4: Print Head Design

In order to achieve in situ curing of the resin, ultraviolet lasers were placed in close proximity to the extrusion point of the material. These lasers were aimed at the center of the extrusion point, with the nozzle tip being adjustable vertically to align the extrusion point with the area of highest UV intensity. Several prototypes were 3D printed out of PLA and tested on the printer to ensure the system would work. One of these prototypes is shown in Figure 12.

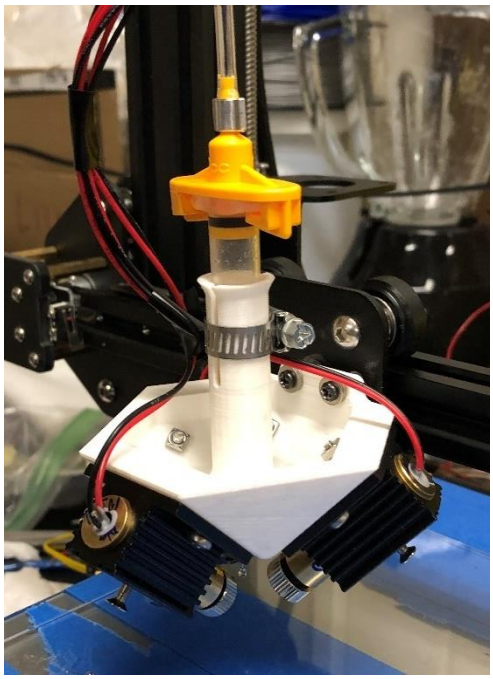

Figure 12: Image of final 3D printed prototype print head mounted on printer

The final version of the print head was machined out of 6061-T6 aluminum in order to more precisely align the lasers and allow for better adjustability. This version added the ability to finely adjust the syringe height by rotating a lead screw and used a jam nut to lock it in place. This method was much better for adjusting the syringe height relative to the lasers. The alignment of the lasers to focus on the same point was also improved due to the higher precision of the machined part. This print head was designed to accept 3 mL Luer-lock syringes. The print head could use these syringes on their own with a pneumatic syringe adapter as a direct ink write printer, or it could use the syringes with the fiber chamber discussed in Section 2.5 to print continuous fiber-reinforced parts.

The lasers used were 1.5-watt 405 nm ultraviolet LED lasers. Three lasers were used in order to ensure that the resin was being cured more evenly, regardless of the direction the print head was moving. The lasers were aimed down towards the extrusion point at a 45° angle. The voltage

regulator was added in order to adjust the laser voltage from 2-5 V to alter their intensity. An image of the completed print head is shown in Figure 13, with a syringe and syringe adapter mounted.

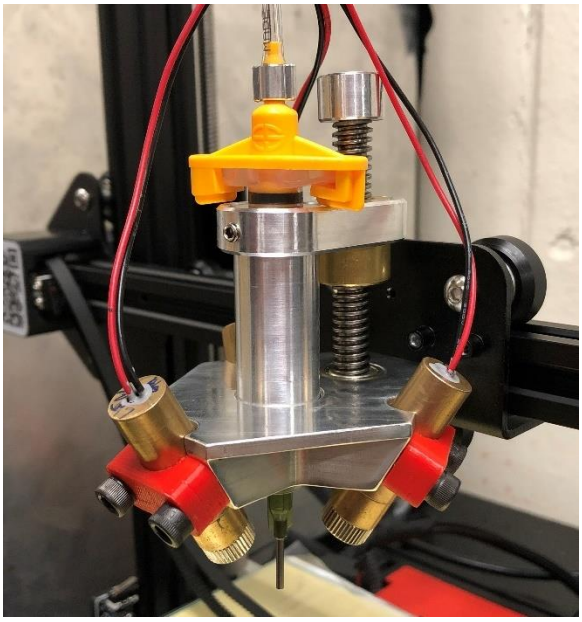

Figure 13: Image of completed print head assembly installed on printer

The focusing lenses were removed from the lasers so that the light was not focused on a point but spread out to a larger area. This helped the lasers to cure larger areas of the print, rather than focusing on a single point. Since the light covered a larger area including the nozzle itself, a shield was made to prevent the material from curing directly on the tip and clogging the nozzle. This shield was 3D printed out of PLA plastic and simply slid over the nozzle tip to block the light. A CAD image of this shield is shown in Figure 14.

Figure 14: CAD image of syringe with laser shield attached

The printer was also able to function well without this shield. For continuous fiber printing, clogs were prevented since the fiber was pulled through the nozzle, ensuring that any material partially cured on the tip was pulled off the nozzle by the fiber. In doing so, the fiber often dragged small pieces of cured material with it as it came out, resulting in a poor top surface finish. Adding the nozzle shield prevented this from happening, and resulted in a smooth, consistent surface finish. Since the prints were all completed on a glass substrate, the bottom surface for each printed sample was very smooth. Although the surface finish was negatively affected, removing the nozzle shield resulted in slightly greater accuracy since the resin was always curing immediately upon extrusion rather than having a delay. With this delay, as the fiber was pulled by the nozzle tip it would drag away from the intended print path around curves in the print. Since the nozzle tips and syringes were translucent, all prints required a cover to prevent light from curing material inside the exposed parts of the syringe. This cover is shown in Figure 15.

Figure 15: CAD image of syringe with cover attached

As seen, this shield did not prevent light from reaching the nozzle tip, but simply acted to prevent premature curing in the syringe.

2.5: Continuous Fiber Chamber Design

In order to print continuous fiber, a chamber was designed and built which would hold the fiber before it was pulled through the resin. Since the system needed to apply pressure to the resin to extrude it, the fiber chamber also needed to be held under pressure. The chamber was built around a clear polycarbonate tube, which was chosen in order to see the amount of fiber left as well as if any tangles occurred which would cause print failures. At the top of the chamber was a metal adapter so that a plug with a rubber O-ring could be screwed in to seal the chamber. The plug was a threaded cap with a hollow tube in the center for the fiber to be wrapped around. The tube was hollow to allow air flow from a pneumatic 4 mm push-to-connect fitting in the plug down into the chamber and out into the syringe. At the bottom of the chamber was a built-in syringe adapter. This adapter had an O-ring on the stem going into the syringe itself. It also had a small bracket which bolted on to the adapter with two screws in order to prevent the syringe from sliding off when pressurized. A cross-sectional CAD image of this assembly is shown in Figure 16.

Figure 16: Cross-sectional CAD image of full fiber chamber assembly

Since the chamber was placed under no more than 60 kPa, there were no safety concerns regarding the chamber. The various parts of the assembly were held together using a two-part epoxy in order to adequately seal and bond the pieces together. The completed assembly is shown in Figure 17.

Figure 17: Image of completed fiber chamber with syringe attached

The completed fiber chamber mounted to the printer by simply sliding the syringe into the print head. The syringe was held tightly enough to hold the entire fiber chamber in place during prints.

2.6: Post-Curing Chamber Design

Once the prints were completed on the printer, they were post-cured to further solidify the resin. To do this, a post-curing chamber was designed and built to allow the samples to be fully exposed to high intensity UV light. Figure 18 shows the completed chamber.

Figure 18: Image of completed UV post-curing chamber

The chamber featured two 405 nm wavelength UV lamps fixed directly above and below the sample. The samples were placed on a glass Petri dish and slid through the opening on the front, where they sat over an opening to allow light to fully the cure samples from the top and bottom. Reflective metal tape covered the inside walls so that light was reflected and helped cure the sides of the print as well. The entire chamber was covered in tape in order to prevent UV light from coming out.

2.7: Printing Process

The novel CFDW process worked by applying air pressure to the resin in order to extrude it out of the syringe. As the resin flowed out, it pulled the fiber with it due to friction, extruding both

materials simultaneously. The UV lights cured the resin in place immediately upon extrusion, hardening around the fibers. A schematic of this process is shown in Figure 19.

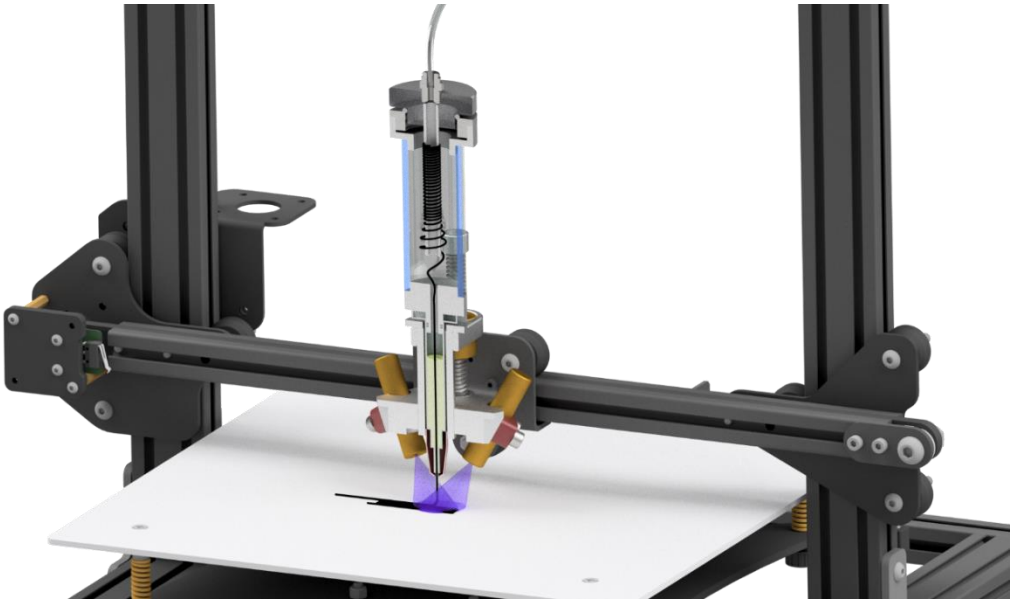

Figure 19: Cross-sectional schematic of CFDW printing process

An up-close image of a sample being printed is shown in Figure 20.

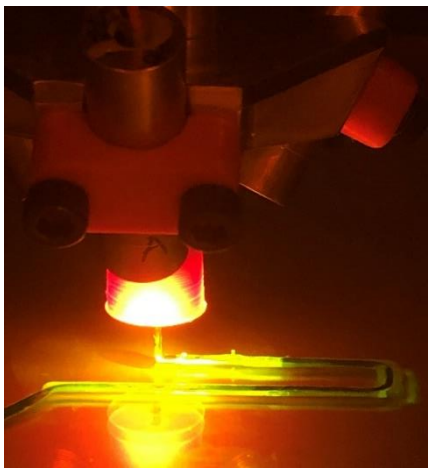

Figure 20: Image of printer creating a sample

This image shows the line width test being printed. The nozzle shield can be seen blocking the UV light from the area just around the needle tip. This image was taken behind the orange light filter of the enclosure, which is why the light appears yellow rather than violet.

CHAPTER 3: SAMPLE PRINTING

3.1: Material Selection

The materials involved in this project were carbon fiber tow and UV-curable 3D printing resin. Carbon fiber was chosen as the fiber material due to its high strength-to-weight ratio and availability to purchase in a roll. Other fibers such as fiberglass or Kevlar were more costly to purchase in rolls of tow and were less commonly used in 3D printing. The fiber came on a large spool, such as that shown in Figure 21, where it was unwrapped and re-spooled into the fiber chamber to print.

Figure 21: Roll of 3k carbon fiber tow [58]

In order to achieve the best print resolution possible, the syringe tip size was reduced to minimize the internal diameter (ID). This was limited by the fact that in order to initially feed the fiber through the syringe tip, the fiber had to be attached to a sewing needle and passed through the syringe tip, resulting in a minimum syringe tip size of 18 gauge (0.838 mm ID) [59]. The length of these syringe tips was approximately 12.7 mm. The length and diameter of the tip had a large effect on the pressure required to flow liquid through the needle. If the nozzle were to drip resin

with no pressure applied, the length could have been increased, or the diameter decreased, in order to increase the force required to induce material flow. The resin used was viscous enough, however, that the material did not drip at this nozzle size. The needle tip used is shown in Figure 22. The needles had Luer-lock threads to easily screw onto the syringes.

Figure 22: 18 gauge Luer-lock syringe tip [60]

The resin used for printing was commercially available Colorado Polymer Systems PR-48 resin. This resin was initially formulated by Autodesk for use with the Autodesk Ember 3D SLA printer, and is shown in Figure 23 [61].

Figure 23: PR-48 Standard Clear photopolymer resin [62]

This material was chosen due to its open-source formulation, common availability, and ability to cure under the 405 nm wavelength provided by the lasers.

3.2: Printer Setup

The printing process worked by first wrapping the continuous fiber onto the spool of the fiber chamber and screwing the spool into the chamber to seal it. The end of this spool was fed out of the chamber and through an empty syringe and dispensing needle. This step only needed to be repeated when the fiber depleted. If the resin ran out first, the syringe could simply be refilled. If the fiber broke in the syringe, a new syringe and dispensing needle would be required so that the fiber could be threaded through the dry needle. Once the fiber was fed through the empty syringe and needle, the resin was placed in the syringe using a pipette. The syringe was then attached to the fiber chamber and fastened in. Figure 24 shows the fiber chamber set up and ready to be placed onto the print head.

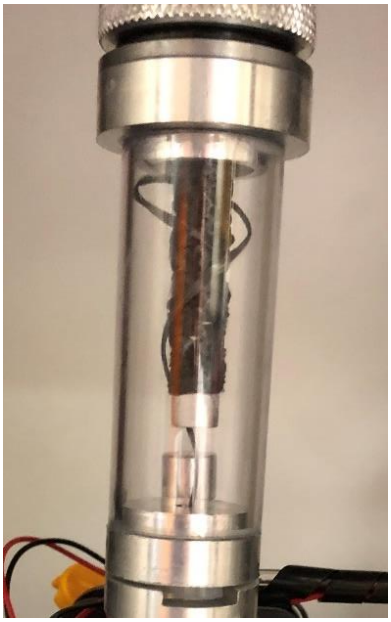

Figure 24: Image of carbon fiber wrapped onto spool and set up on printer

The entire fiber chamber assembly was then placed onto the print head, and the tubing from the pneumatic system was attached to the chamber. Lastly, the nozzle shield was attached to the syringe, and the print head assembly was ready.

The next step was to set the gap between the lasers, tip, and plate. First the lasers were turned on and brought to the Z-height where they were focused on the same point. This value was read on the dial indicator. Then, the gap from the syringe tip to the laser center point was set by lowering the syringe tip to the desired location using the adjustment lead screw on the print head. This step only needed to be completed once. Then, for every print, the gap from the needle tip to the print bed (which determined the base layer thickness) was set by touching the tip to the bed, reading the value on the dial indicator, and then raising the print head up by desired base layer height. Once this was set up, any changes to the air pressure and laser voltage could be made. These parameters only needed to be changed as needed for each print. The printer was then fully set up and ready to print.

3.3: Processing Parameters

There were many parameters to be considered, as with any additive manufacturing process. In order to fine-tune these parameters, they were initially varied starting with the most important and working towards the least important. The printing processes were repeated until the printer was able to produce satisfactory samples by progressively fine-tuning several parameters including the extrusion pressure, print speed, laser intensity, etc. The most important of these printing parameters are described in the following subsections.

3.3.1: Extrusion Pressure & Feed Rate

The most important aspect of achieving a high print quality was to characterize the relationship between the extrusion pressure and feed rate. Extrusion pressure describes the air pressure applied to the resin, which affected the flow rate of resin out of the nozzle. Feed rate describes the speed at which the print head moved in the XY-plane. In order to print successfully, a balance had to be achieved between these two parameters. For example, a low feed rate required a low extrusion

pressure or to avoid excess resin flow, while a high feed rate required a high extrusion pressure to have sufficient resin flow.

This relationship was complicated by the fact that the fiber extruding out of the syringe tip affected the flow rate of resin. While moving in a straight line, the fiber exited the syringe at a rate equal to the feed rate of the printer. This resulted in a more complex relationship in which the rate of resin flow could not be easily calculated. Since the fiber was coated with the resin as it came out of the syringe, the printer could print the fiber with no pressure applied. This was possible because the fiber stuck to the build plate as the resin was cured, and it was pulled out of the nozzle as the print head moved. While the printer could print in this way, it resulted in an asymmetric and insufficient coating of the fiber, as the top layer of resin was scraped off as the fiber exited the syringe. In contrast, the extrusion pressure could also be set too high for the given feed rate. In this case, the fiber was laid down normally, but the resin flowed out more around the fiber. This resulted in a very large and uneven coating of resin. Another consideration to be made with these parameters was that the quicker the speed, the less exposure time there was for the lasers to cure the material. This meant that it was generally better to choose a slower feed rate and lower pressure even though quicker prints were possible.

3.3.2: Layer height & Hatch spacing

The next most important printing parameters were the layer height and hatch spacing. Layer height describes the vertical distance between layers, while hatch spacing describes the horizontal distance between printed lines. Figure 25 shows a schematic of this relationship.

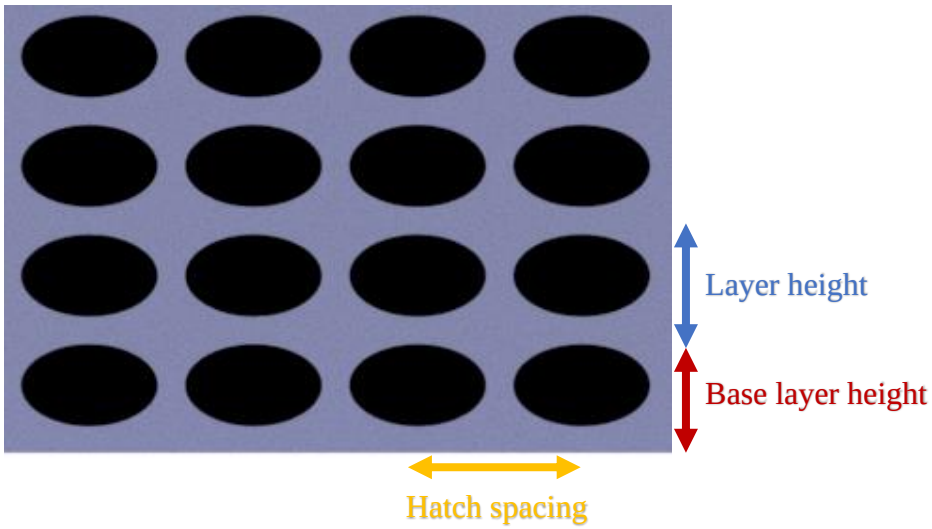

Figure 25: Illustration showing hatch spacing and layer height

The layer height could be set to any value from approximately 0.5 mm to 1 mm. As the nozzle moved across the part, it laid the fiber down and the resin predominantly flowed radially in relation to the vertical syringe axis. This meant that the layer height was not greatly affected by other parameters but was simply set by the starting height and g-code. It was found that the base layer adhered best at a layer height of 0.5 mm, so this value was used for all the test prints. Bulk samples were printed with this base layer height of 0.5 mm and subsequent layer heights of 0.8 mm. This value was kept at a minimum in order to increase the fiber volume fraction.

The hatch spacing was largely dependent on the extrusion pressure, deposition speed, layer height, and nozzle size. All these parameters affected how much resin flowed radially, which set the hatch spacing. From testing this experimentally, it was found that 1.2 mm was the lowest this value could be, as the nozzle itself (18 gauge needle) had an outer diameter of 1.27 mm and would deflect under smaller hatch spacings [59]. The hatch spacing also was minimized to increase the fiber volume fraction.

3.3.3: Laser Parameters

Each of the test prints was carried out with the same laser settings. Three 405 nm wavelength LED lasers were aimed directly at the center of the extrusion point at a 45° angle. Each laser was a 5V, 1.5W laser but was only powered at 3V in order to reduce the intensity and slow the curing time slightly. These parameters were still sufficient to cure the resin almost immediately upon extrusion. Although these parameters were not varied in these experiments, they would be important factors to study further as they affected the rate and extent of the cure. The prints were also post-cured in the UV-curing chamber for 20 minutes in order to further cross-link the polymer.

3.3.4: Other Parameters

Among the various other parameters which could be altered, three of the most important were nozzle size, fiber size, and material viscosity. Nozzle size was minimized in order to reduce hatch spacing and improve the print resolution, with the drawback of increased print time. The fiber size was dependent on the nozzle size, as the more it filled of the internal diameter, the easier it was to be pushed out as the resin flowed. T300 carbon fiber 3k tow was chosen for this purpose. Smaller carbon fiber such as1k tow would have resulted in a small fiber volume fraction, and 6k tow would have likely torn as the fibers scraped the needle tip. Material viscosity could also be altered with additives or by varying temperature to change the flow characteristics. The viscosity of the resin as determined by the manufacturer was 300 centipoise [63]. Altering the viscosity of the resin would affect the flow out of the nozzle as well as change its ability to penetrate the fiber tow.

3.4: G-Code Generation Using MATLAB

The g-codes used to manufacture sample prints were created using various MATLAB programs developed to take input parameters regarding sample geometry and to export g-code for the printer. While the g-codes were very similar to those created by a normal slicer, the use of continuous fiber dictated that the print path be continuous. It was therefore easier to create simple programs for print paths which would need to be altered often. Three main programs were created for the samples: one which created bulk rectangular shapes, one which created hollow cylindrical and conical shapes, and one which followed a set of coordinates. The program used most often was for creating bulk rectangular samples. The inputs to this program are shown in Figure 26.

```
%%%%%%%%%%%%%%%INPUTS%%%%%%%%%%%%%%%

filename        = "box"     ; %name
width           = 12        ; %mm
length          = 50        ; %mm
layers          = 3         ; %layers
step            = 1.2       ; %mm
feed_rate       = 1         ; %mm/s
xrun_in         = 10        ; %mm
yrun_in         = 10        ; %mm
layer_height    = 0.8       ; %mm

%%%%%%%%%%%%%%%%%%%%%%%%%%%%%%%%%%%%%
```

Figure 26: Input parameters for MATLAB program

This program took the width, length, height, stepover, layer height, and feed rate desired and exported the g-code. When the program was run, it exported a g-code file which could be uploaded directly to the printer. Figure 27 shows the results of opening the g-code file with the parameters

from Figure 26 in the 3D printing software Repetier-Host. This program was used to create the samples made in Sections 4.1-4.5.

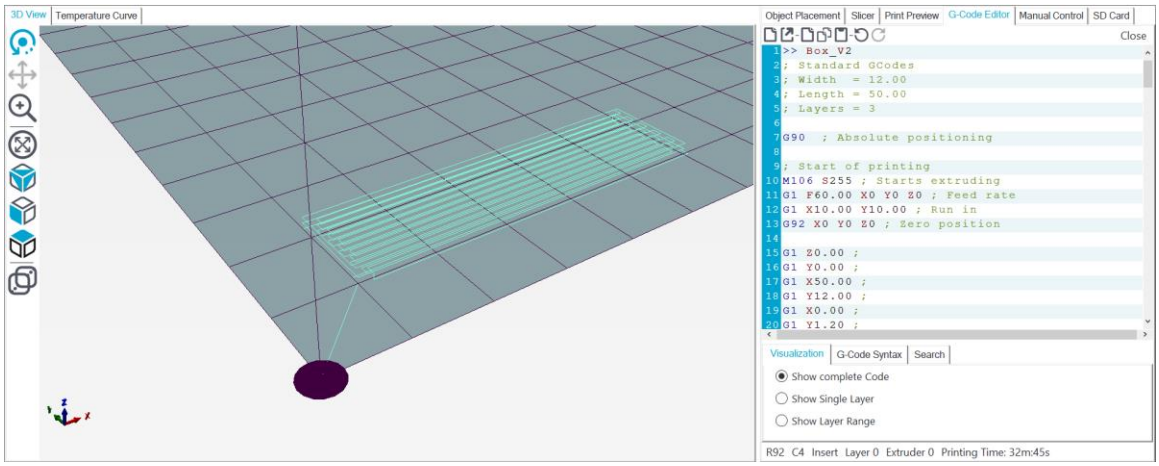

Figure 27: Repetier-Host screenshot showing the output file from the MATLAB code

The program for creating cylinders and cones was used to create more complex samples. This program took the base diameter, tip diameter, height, number of coils, feed rate, and resolution as inputs. The resolution affected how many vertices would lie on a circle, so using a small number of vertices resulted in the creation of a polygon, but as the number increased it approximated to become a circle. This program was used to create the print path for the sample created in Figure 48. The last created program followed coordinate points from a given .txt file, and could alter the number of layers, layer height, and feed rate. It also had the ability to scale and translate the coordinates as needed. This program was useful for creating more complex shapes, such as the airfoil in Figure 47.

3.5: Sample Processing

The first samples created were simple lines used to characterize the width of a printed line, followed by single and multilayer bulk rectangles. To achieve this, one layer of the pattern was printed using g-code created from the MATLAB program described in Section 3.4. The rectangles

were completed with either a single layer to characterize the base layer, or multilayer to characterize a bulk sample. Complex samples were also printed in order to demonstrate the capabilities of the printing process. These samples included a horizontal overhang test, vertical printing test, complex print path, hollow airfoil structure, and hollow cone structure. These results are further discussed in Chapter 4.

CHAPTER 4: SAMPLE ANALYSIS

4.1: Line Width Measurements

One of the most important parameters for achieving a high print quality was to determine the relationship between the print speed and extrusion pressure. By varying these two parameters, the width of a single printed line varied significantly. These parameters affected how much resin flowed out and covered the fiber, which therefore affected the fiber volume fraction of a single line. Information regarding the width of each line was also an important factor for setting the hatch spacing of multi-line prints. In order to test this relationship, single lines were printed at speeds ranging from 0.5 mm/s to 2 mm/s and at pressures ranging from 0 kPa to 50 kPa. Table 4 shows the printing parameters used in this study.

Table 4: Printing parameters for line width tests

Parameter	Value
Feed rate	0.5, 0.75, 1, 1.25, 1.5, 1.75, & 2 mm/s
Extrusion Pressure	0, 10, 20, 30, 40, & 50 kPa
Base layer height	0.5 mm
Number of layers	1

A single sample was printed for each pressure, with the speed increasing progressively during the print. The print pattern is shown in Figure 28. Each vertical line in the print path is printed at a different speed.

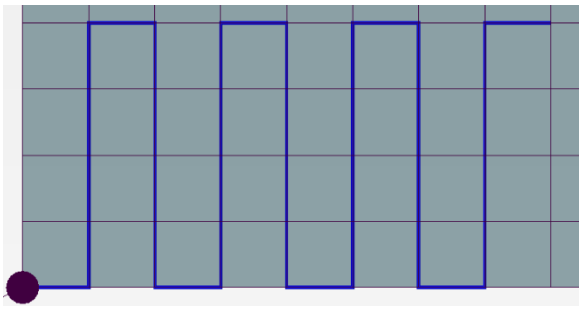

Figure 28: Print path for line width tests

The nozzle height relative to the bed was held constant for each test. This was important because it ensured a consistent base layer height, meaning that all the resin flowing out was doing so in the radial direction relative to the nozzle. A printed sample is shown in Figure 29.

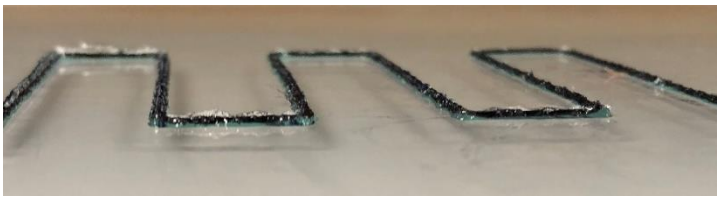

Figure 29: Resulting sample printed to measure the line widths

The cross-section of each line did not have a constant width. They tended to be wider at the base, where each measurement was taken. Figure 30 shows an illustration of this cross-sectional shape.

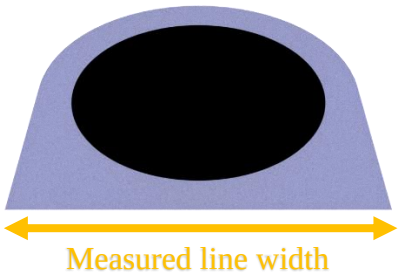

Figure 30: Illustration of a typical cross section of a single printed line

Once each print was complete, the width of each line was measured, with the sample still on the print bed, using dial calipers. Measurements were taken near the beginning, middle, and end of each line. Figure 31 shows the average values for these results.

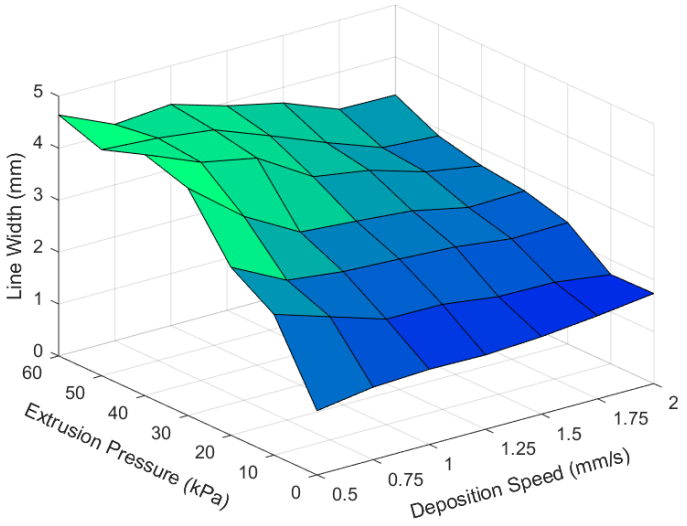

Figure 31: Line width as a function of deposition speed and extrusion pressure

As seen in the figure, both speed and pressure dramatically affected the width of a single printed line sample. As expected, having a high pressure with a low feed rate resulted in a large line width with excess resin, while having a low pressure with a high feed rate resulted in a small line width.

Also of note in this experiment was the relationship of line width vs feed rate at 0 kPa. With no applied pressure, all the resin that came of the nozzle was pulled by the fiber itself. As the feed rate was increased, the fiber was pulled out of the nozzle more quickly, which resulted in more resin flow as well. This was why there was an increase in line width for an increase in feed rate at zero applied pressure.

4.2: Effect of Extrusion Pressure on Print Quality

To further study the effects of extrusion pressure and deposition speed, both parameters were tested independently. Single-layer rectangular samples were printed at a constant speed in the path shown in Figure 32.

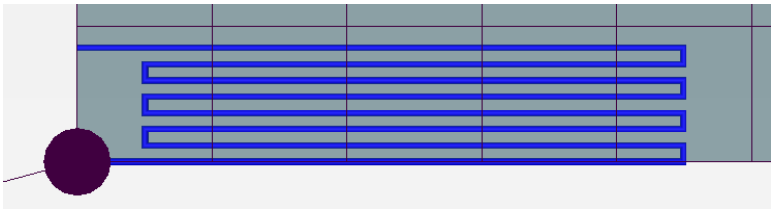

Figure 32: Print path for constant feed rate tests

The print parameters for these tests are shown in Table 5.

Table 5: Printing parameters for constant feed rate tests

Parameter	Value
Feed rate	1 mm/s
Extrusion Pressure	10, 20, 30, 40, & 50 kPa
Base layer height	0.5 mm
Hatch spacing	1.2 mm
Number of layers	1

The first goal of these samples was to see if any significant changes in top surface quality were found. The top surface of each sample is shown in Figure 33. Since all samples made with this printer were printed on the same glass print bed, the surface was extremely smooth on the bottom and was therefore not studied.

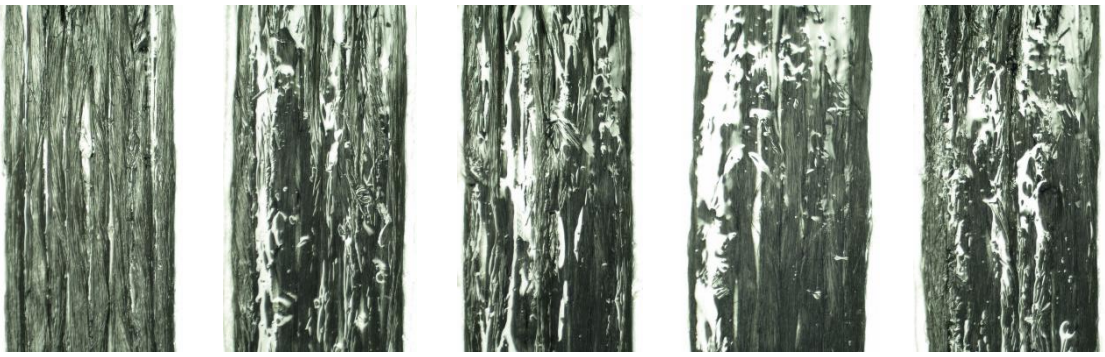

10 kPa 20 kPa 30 kPa 40 kPa 50 kPa

Figure 33: Top surface finish results from varying extrusion pressure

The results of this study were that the surface was high quality for each of the samples. This was because the resin flowing out filled gaps between adjacent lines and resulted in a smooth surface. The second goal was to get an adequate coating of the fibers in each layer. Figure 34 shows cross-sectional images of each sample.

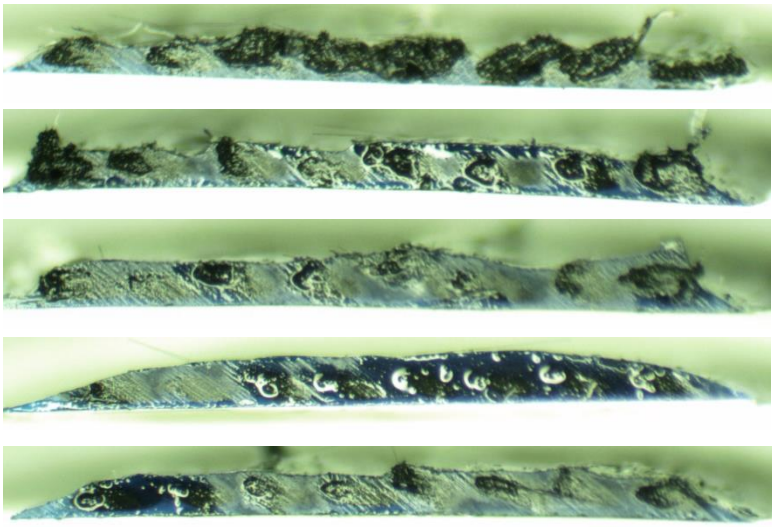

Figure 34: Cross-sectional images of samples with varying extrusion pressure

As seen in the figure, at high extrusion pressures the resin coated the fiber much more than at lower extrusion pressures. This resulted in a thicker layer, but also a more consistent coating of the layer. The samples printed at the lower pressures were not sufficiently coated with resin and resulted in very fragile samples.

It was also found in this experiment that the fiber and resin require a certain pressure to begin flowing out on their own. This was tested by holding the print head well above the print bed and finding the pressure at which the material would begin to extrude. At pressures below 30 kPa, the fiber did not extrude from the nozzle on its own. This meant that the fiber was dragged out of the nozzle by the portion adhered to the print bed as the print head moved. At pressures of 30 kPa or above, the pressure was enough to force the materials to flow out on their own. This was the

preferred condition, as it was less likely to tear fibers if the fibers were not pulled against the sidewall of the nozzle as it extruded.

4.3: Effect of Feed Rate on Print Quality

The effects of varying feed rate were also studied independently of extrusion pressure. Since pressure was not being varied, samples could be printed on the same build plate. The print path for these samples is shown in Figure 35.

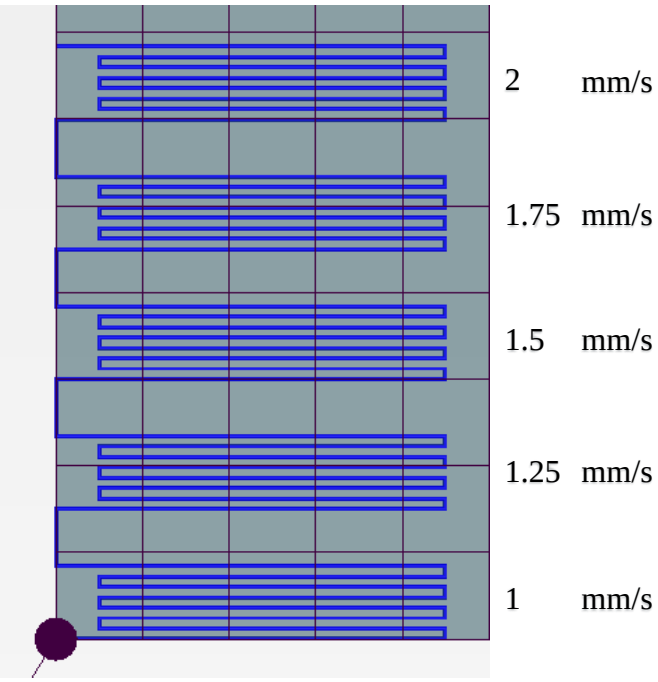

Figure 35: Print path for constant pressure tests

The print parameters for these tests are shown in Table 6.

Table 6: Printing parameters for constant pressure tests

Parameter	Value
Feed rate	1, 1.25, 1.5, 1.75, & 2 mm/s
Extrusion Pressure	30 kPa
Base layer height	0.5 mm
Hatch spacing	1.2 mm
Number of layers	1

The completed print is shown in Figure 36.

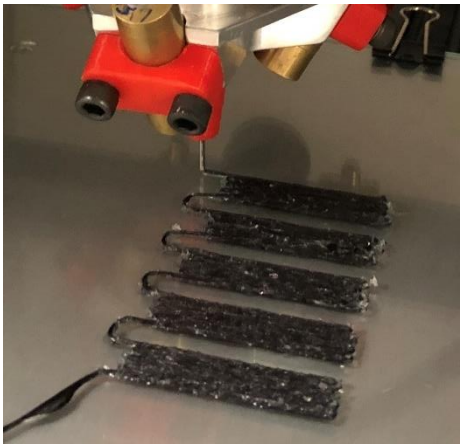

Figure 36: Completed print for constant pressure tests

As with the constant speed tests, the first goal was to see if any significant changes in surface quality were found. The top surface of each sample is shown in Figure 37.

Figure 37: Top surface finish results from varying feed rate

The results of this were that, like the previous test, the surface was only minimally affected. The resulting surfaces were consistent and smooth regardless of the feed rate. The second goal was to see the coating of the fibers in each layer. Figure 38 shows cross-sectional images of each sample.

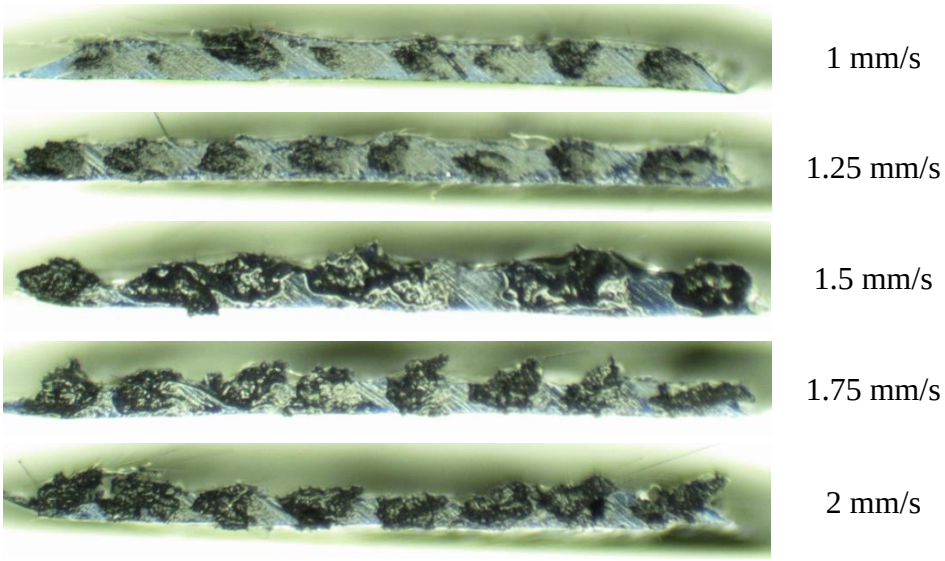

Figure 38: Cross-sectional images of samples with varying feed rate

As seen in the figure, at low feed rates the resin coated the fiber much more than at higher feed rates. This resulted in a thicker layer, but also a more consistent coating of the fiber. The samples printed at the higher feed rates were not sufficiently coated and resulted in very fragile samples with exposed fibers on the top surface.

4.4: Cross-sectional Imaging of Multilayer Samples

In order to analyze the voids and fiber volume in bulk samples, a multilayer sample was printed and the cross-section was imaged. A five-layer rectangular sample was created for this purpose, as seen in Figure 39.

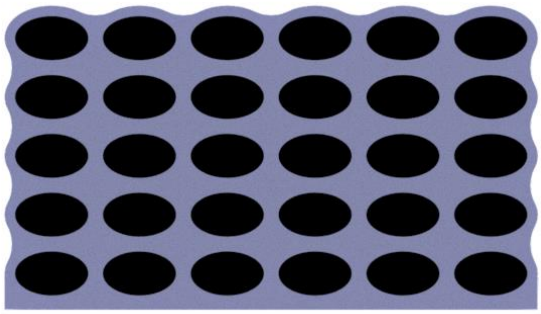

Figure 39: Illustration of rectangularly stacked tow cross-section

This print was carried out at 30 kPa and 1 mm/s, which was found in the line width experiments to provide a consistent amount of resin. Table 7 shows the full print parameters.

Table 7: Printing parameters for multilayer sample tests

Parameter	Value
Feed rate	1 mm/s
Extrusion Pressure	30 kPa
Base layer height	0.5 mm
Hatch spacing	1.2 mm
Number of layers	5
Layer height	0.8 mm

The resulting cross-sectional image for this sample is shown in Figure 40.

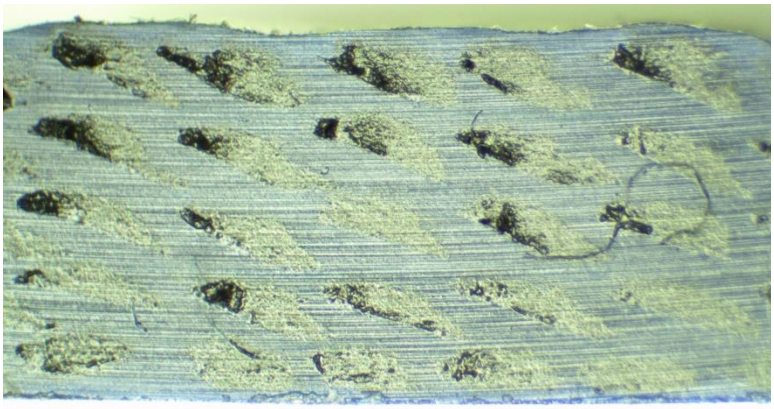

Figure 40: Cross-section of 5-layer rectangularly stacked sample

There were multiple conclusions to be made from this image. The first was that the narrow hatch spacing caused the lines to be slightly slanted. As the print moved from the left to the right on each layer, the printed fiber stacked partially on top of the adjacent printed line. The second realization from this was the void content. While there were no large voids seen in the matrix, the tows themselves had regions in which the resin did not fully cure, resulting in loose fibers (seen as the darkest areas of the fiber in Figure 40). This was an issue which could likely be fixed with better printing parameters, as it did not occur in every tow, and occurred less often in those where the tows were more flattened.

An estimate for the fiber volume fraction was found using the image analysis software ImageJ. The fiber volume fraction was estimated by assuming the fibers were densely packed together. This resulted in a fiber area shown in Figure 41, where the black areas (excluding the area above and below the sample) were assumed to be carbon fiber. The software measured the area of each of the tows and that of the entire sample. Dividing the total area of the tows by the total area of the sample gives an estimate for the fiber volume fraction.

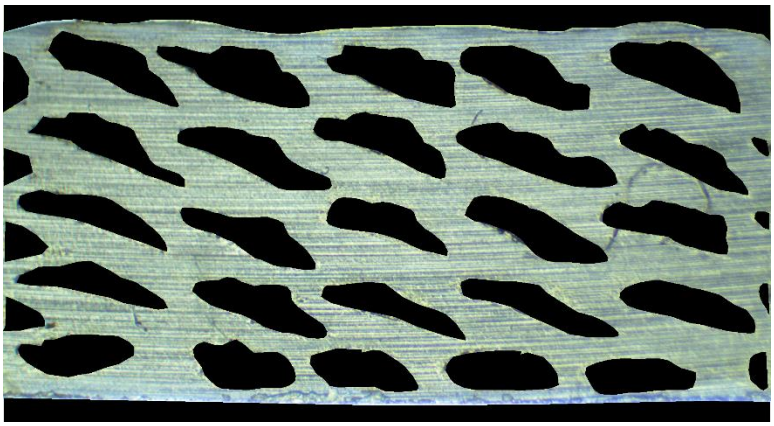

Figure 41: ImageJ analysis of fiber volume

From this, the fiber volume fraction was found to be approximately 37%. Since this approximation was made assuming there was no resin within each tow, it was an overestimate. Although the void fraction could theoretically be calculated in this same way, the images did not have high enough resolution to differentiate the voids from the cured areas within each tow.

4.5: Samples without Nozzle Shield

In each of the previous samples mentioned, the nozzle shield was placed on the nozzle so that the UV light from the lasers was blocked immediately surrounding the nozzle. This was done in order to prevent clogging of the nozzle to improve the surface finish. Several prints were completed, however, without the nozzle shield. A comparison of samples printed with and without the nozzle shield are shown in Figure 42.

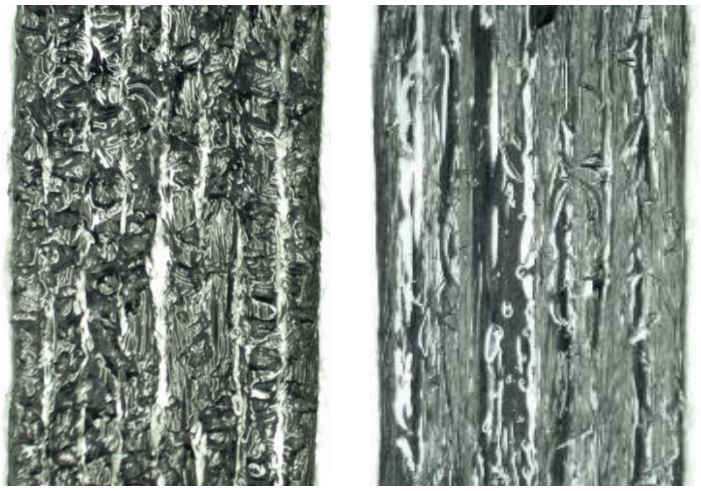

Not shielded Shielded

Figure 42: Sample printed at 30 kPa and 1 mm/s with and without nozzle shield

Similar tests were carried out as in Sections 4.2 and 4.3 to characterize the surface improvements and resin distribution. It was found from these experiments that the surface quality appeared better as less resin was used (i.e. less extrusion pressure or higher feed rate). From examining the cross-sections, however, it was found that the surface only appeared better because there was less resin in total. This phenomenon was likely due to the partially clogged nozzles producing a poor surface finish. Excess resin was necessary to achieve any strength in the prints. This meant that the samples with a smooth surface finish were very fragile and were actually much lower quality than their counterparts printed with the nozzle shield.

Printing samples without the nozzle shield was beneficial in some cases due to its improved dimensional accuracy. Since the resin began to cure immediately as it exited the nozzle, the printer could print more accurate turns and curves. This extra curing time immediately out of the nozzle resulted in the fiber being laid down closer to the actual print path rather than dragging further away as the curing was delayed. With an improved nozzle shield, it would be possible to minimize the delay in curing while still preventing nozzle clogs during the print.

4.6: Complex Samples

Several more complex objects were printed to demonstrate the capabilities of the CFDW printing method. First, a 150 mm line was printed horizontally through free space without support to show its ability to span a gap. This is shown in Figure 43.

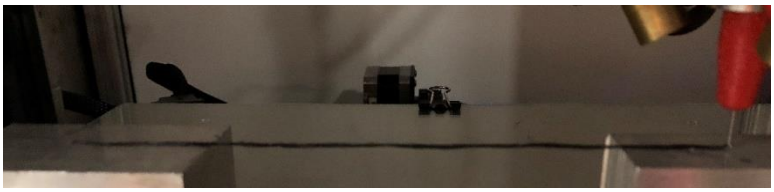

Figure 43: Print spanning 150 mm gap with no support

This method worked under the conditions that the pressure was low and the feed rate was high. This way the fiber was held in tension by the nozzle and pulled out as the print head moved until it reached the other side of the gap. A larger gap could likely be spanned in this method with a larger print bed.

A 100 mm vertical line was also printed, to show the printer's ability to print vertically. This is shown in Figure 44.

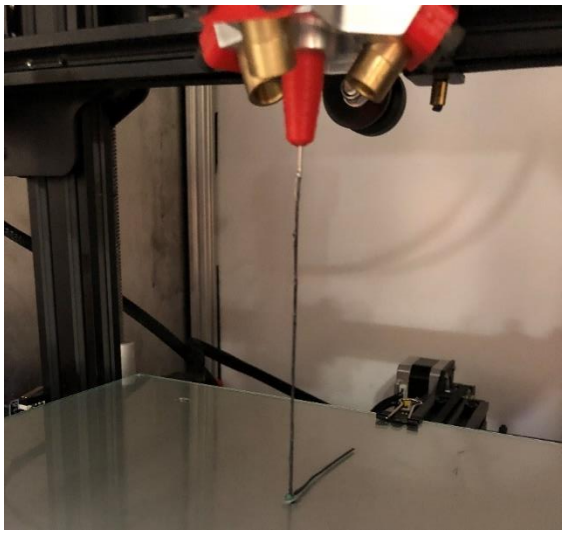

Figure 44: Vertical line printed 100 mm high

As with spanning the gap, this method required low pressure applied so that the fiber could be pulled out of the nozzle and held in tension to remain straight and upright. Likewise, a longer fiber could likely be printed without issue.

To demonstrate the ability of the printer to print sharp turns, a complex print path was tested. Figure 45 shows the print path.

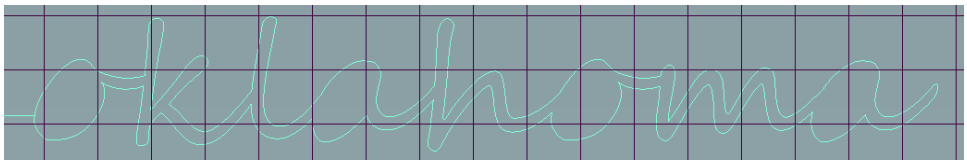

Figure 45: Print path of text spelling the word "Oklahoma"

The completed print is shown in Figure 46.

Figure 46: Complex print path outlining the word "Oklahoma"

As seen, the print was able to complete the print path relatively well. Sharp corners result in the fiber dragging slightly, but larger radii gave good accuracy. There were also some slight tears in the fiber at the sharp turns, seen where the tow split apart in Figure 46.

A hollow airfoil structure was also printed to demonstrate the printer's capabilities to print a complex shape in multiple layers. The resulting airfoil is shown in Figure 47.

Figure 47: Completed hollow airfoil structure

Lastly, a hollow cone was printed to show the ability to print more than a single slice stacked on top of itself. The cone is shown in Figure 48.

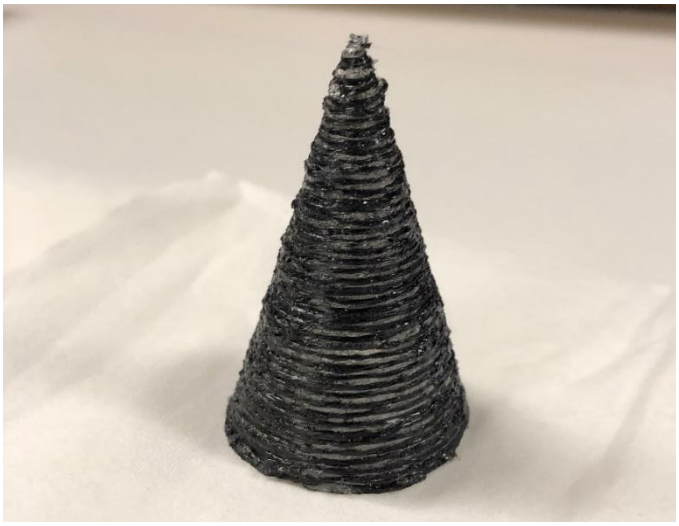

Figure 48: Completed hollow cone structure

This cone was a single layer thick, 45-layer tall structure. This shows the ability of the printer to print overhangs without the need for support material underneath. This structure was not printed in separate layers, but instead spiraled up as it printed.

CHAPTER 5: CONCLUSIONS AND FUTURE WORK

The development of the CFDW method was shown to be a viable additive manufacturing method for creating continuous fiber-reinforced thermosetting 3D prints. In order to create continuous fiber AM samples, an existing FDM printer was heavily modified with a custom print head and extrusion system to extrude fiber and resin out of a syringe. This was achieved through the creation of a pneumatic system which applied pressure at the top of the syringe to push material out. To effectively operate the printer, custom MATLAB programs were created which could make continuous print paths and quickly adjust the geometric parameters of those paths. Once the printer was operational, several printing parameters were tested in order to improve the print quality. These factors included deposition speed, extrusion pressure, nozzle size, nozzle-plate gap, and laser intensity. The primary goal of this was to achieve consistency in printing so that the parts would have accurate geometry and minimal print failures. Once initial parameters were set which could consistently create samples, deposition speed and extrusion pressure were studied more in depth in order to improve the surface finish and strength of the completed samples.

Through studying the deposition speed and extrusion pressure it was found that the width of a single line increased with either a decrease in deposition speed or an increase in extrusion pressure. This meant that these two parameters needed to be balanced in order to achieve a desired line width. The surface finish and fiber coating were more closely examined in sample sets with varying extrusion pressure or deposition speed. It was found in both studies that surface finish was only minimally affected, but that the fibers would not be sufficiently coated at high deposition speeds or low extrusion pressures. Using these studies, a five-layer sample was printed using the best-known printing parameters. An analysis of the cross-section using image analysis software found that the fiber volume fraction was approximately 37%. This value could likely be improved

through fine-tuning the printing parameters. The printer was also able to manufacture several complex shapes to prove its capabilities, including complex print paths and multilayer hollow structures.

The main issues encountered in printing samples were nozzle clogs and lack of bed adhesion. The nozzle clogging issue was solved through the addition of a nozzle shield so that light would not cure resin immediately surrounding the extrusion point. This resulted in a slight reduction of print accuracy but created better samples overall with drastically improved surface finish and fiber coating. The lack of bed adhesion was solved through adjusting the base layer height and tuning the print parameters so that the resin cured in an appropriate time in relation to deposition speed. Through studying the feed rate and extrusion pressure, parameters were found which could print dense multilayer samples with minimal voids and a good surface finish.

Further research into this project would start with a parameter study of some of these other factors that were not altered throughout these experiments. These include such things as UV intensity, fiber material, fiber size, nozzle size, resin viscosity, etc. Testing other fibers such as Kevlar or glass would also be a way to increase the toughness or reduce the cost of these samples. Mechanical testing would also be an important aspect to study, as even without changing materials, simply altering the various parameters could increase the fiber volume fraction which would have a large effect on the mechanical properties. It could also be beneficial to use a stronger thermally curable epoxy resin with some amount of photoinitiator in it. This way, the UV-curing could be used to give the part the necessary strength to complete the print, and thermal post-curing could fully strengthen the part to a very high strength.

The area of study which would be the most impactful with this printer would be to study the effects of controlling the fiber direction. By 3D printing the continuous fibers, the direction could be

printed such that it would follow the geometry of the part (i.e. as it comes to a hole it bends around it rather than stopping abruptly) which would allow for specific areas to be reinforced. This would reduce stress concentrations and therefore maximize the strength of the part, without adding significant weight or volume. Having these reinforcing fibers throughout the prints could result in parts which are extremely strong in comparison to other 3D printed components. Using strong resins and controlling the direction of the fibers could give this method the possibility of creating some of the strongest and stiffest components found in the field of polymer AM.

Due to the ease at which materials can be altered for the CFDW process, it is possible to further tailor the resin's rheological properties by dispersing nanoscale and transparent particles within the resin. Nanoscale cellulose crystals could be one of the nanoparticles dispersed in the UV-curable resin to increase its viscosity for printing [64, 65]. Other nanoparticles, such as piezoelectric ceramics, graphene, and carbon nanotubes, could also be dispersed in the resin [66-71]. Certain nanoparticles would not only improve the 3D printing capabilities, but also lead to benefits such as improved mechanical, thermal, and electrical properties. Nanoparticles could also allow for self-sensing capabilities for damage detection during long-term service under complex load conditions and harsh environments [72-75].

The developed CFDW printer could also serve as a platform for the investigation of real-time quality assurance. Currently, most 3D printers lack the capability to detect potential material imperfections during the printing process. Quality assurance devices could be installed on the printer to monitor prints in real-time. For example, pulsed laser-induced acoustic emission systems could be included on the printer [76-78]. Ultrasonic signals could be used during the printing process to generate 3D images to identify any voids or fiber misalignment. In addition, many algorithms and technologies developed for structural health monitoring of composite and metallic

structures could be employed for real-time quality assurance during printing [79-85]. Advanced ultrasonic analysis methods, such as time domain analysis, frequency domain analysis, and time-frequency domain analysis, could be employed for the 3D microstructural image generation during printing [86-91]. Additionally, the identification of microscale voids could lead to an analysis of the service life of the 3D printed composites [92-96]. These monitoring systems could not only lead to a better understanding of the quality of the prints, but also provide information regarding the improvement of the printing parameters. This information would assist the continued improvement of the quality of 3D printed composites.

References

[1] T. D. Ngoa, A. Kashania, G. Imbalzanoa, K. T. Q. Nguyena, and D. Huib, Additive manufacturing (3D printing): A review of materials, methods, applications and challenges, *Composites Part B: Engineering,* vol. 143, pp. 172-196, 2018.

[2] K. V. Wong and A. Hernandez, A review of additive manufacturing, *International scholarly research notices,* vol. 2012, 2012.

[3] M. Abshirini, M. Charara, P. Marashizadeh, M. C. Saha, M. C. Altan, and Y. Liu, Functional nanocomposites for 3D printing of stretchable and wearable sensors, *Applied Nanoscience,* vol. 9, no. 8, pp. 2071-2083, 2019.

[4] A. Renteria, J. A. Diaz, B. He, I. A. Renteria-Marquez, L. A. Chavez, J. E. Regis, Y. Liu, D. Espalin, T.-L. B. Tseng, and Y. Lin, Particle size influence on material properties of BaTiO3 ceramics fabricated using freeze-form extrusion 3D printing, *Materials Research Express,* vol. 6, no. 11, p. 115211, 2019.

[5] S. H. Huang, P. Liu, A. Mokasdar, and L. Hou, Additive manufacturing and its societal impact: a literature review, *The International Journal of Advanced Manufacturing Technology,* vol. 67, no. 5-8, pp. 1191-1203, 2012.

[6] B. Hoelzel, Additive manufacturing of HDPE using selective laser sintering, School of Aerospace and Mechanical Engineering, University of Oklahoma, 2019.

[7] L. A. Chavez, B. R. Wilburn, P. Ibave, L. C. Delfin, S. Vargas, H. Diaz, C. Fulgentes, A. Renteria, J. Regis, and Y. Liu, Fabrication and characterization of 3D printing induced orthotropic functional ceramics, *Smart Materials and Structures,* vol. 28, no. 12, p. 125007, 2019.

[8] J. A. Lewis, Direct ink writing of 3D functional materials, *Advanced Functional Materials,* vol. 16, no. 17, pp. 2193-2204, 2006.

[9] S. F. S. Shirazi, S. Gharehkhani, M. Mehrali, H. Yarmand, H. S. C. Metselaar, N. A. Kadri, and N. A. A. Osman, A review on powder-based additive manufacturing for tissue engineering: selective laser sintering and inkjet 3D printing, *Science and technology of advanced materials,* vol. 16, no. 3, p. 033502, 2015.

[10] S. L. Sing, W. Y. Yeong, F. E. Wiria, B. Y. Tay, Z. Zhao, L. Zhao, Z. Tian, and S. Yang, Direct selective laser sintering and melting of ceramics: a review, *Rapid Prototyping Journal,* 2017.

[11] L. A. Chavez, J. E. Regis, L. C. Delfin, C. A. Garcia Rosales, H. Kim, N. Love, Y. Liu, and Y. Lin, Electrical and mechanical tuning of 3D printed photopolymer–MWCNT nanocomposites through in situ dispersion, *Journal of Applied Polymer Science,* vol. 136, no. 22, p. 47600, 2019.

[12] M. Upadhyay, T. Sivarupan, and M. El Mansori, 3D printing for rapid sand casting—A review, *Journal of Manufacturing Processes,* vol. 29, pp. 211-220, 2017.

[13] D. Popescu, A. Zapciu, C. Amza, F. Baciu, and R. Marinescu, FDM process parameters influence over the mechanical properties of polymer specimens: A review, *Polymer Testing,* vol. 69, pp. 157-166, 2018.

[14] A. Renteria, H. Fontes, J. A. Diaz, J. E. Regis, L. A. Chavez, T.-L. B. Tseng, Y. Liu, and Y. Lin, Optimization of 3D printing parameters for BaTiO3 piezoelectric ceramics through design of experiments, *Materials Research Express,* vol. 6, no. 8, p. 085706, 2019.

[15] J. Horvath, *Mastering 3D Printing*. 2014.

[16] B. Wendel, D. Rietzel, F. Kühnlein, R. Feulner, G. Hülder, and E. Schmachtenberg, Additive Processing of Polymers, *Macromolecular Materials and Engineering,* vol. 293, no. 10, pp. 799-809, 2008.
[17] F. Calignano, D. Manfredi, E. P. Ambrosio, S. Biamino, M. Lombardi, E. Atzeni, A. Salmi, P. Minetola, L. Iuliano, and P. Fino, Overview on Additive Manufacturing Technologies, *Proceedings of the IEEE,* vol. 105, no. 4, pp. 593-612, 2017.
[18] A. Rodriguez-Panes, J. Claver, and A. M. Camacho, The Influence of Manufacturing Parameters on the Mechanical Behaviour of PLA and ABS Pieces Manufactured by FDM: A Comparative Analysis, *Materials (Basel),* vol. 11, no. 8, Aug 1 2018.
[19] M. S. Houssain, J. Ramos, D. Espalin, M. Perez, and R. Wicker, Improving Tensile Mechanical Properties of FDM-Manufactured Specimens via Modifying Build Parameters
[20] A. Paesano, Polymeric Additive Manufacturing Present Status and Future Trends of Materials and Processes, *Boeing Technical Journal,* 2016.
[21] A. P. West, S. P. Sambu, and D. W. Rosen, A process planning method for improving build performance in stereolithography.
[22] F. P. Melchels, J. Feijen, and D. W. Grijpma, A review on stereolithography and its applications in biomedical engineering, *Biomaterials,* vol. 31, no. 24, pp. 6121-30, Aug 2010.
[23] D. S. John R. Tumbleston, Nikita Ermoshkin, Rima Janusziewicz, Ashley R. Johnson, David Kelly, Kai Chen, Robert Pinschmidt, Jason P. Rolland, Alexander Ermoshkin, Edward T. Samulski, Joseph M. DeSimone, Continuous liquid interface production of3D objects.
[24] R.-J. Wang, L. Wang, L. Zhao, and Z. Liu, Influence of process parameters on part shrinkage in SLS, *The International Journal of Advanced Manufacturing Technology,* vol. 33, no. 5-6, pp. 498-504, 2006.
[25] I. Gibson, D. Rosen, and B. Stucker, Additive Manufacturing Technologies.
[26] R. Koike, R. Ashida, K. Yamazaki, Y. Kakinuma, T. Aoyama, Y. Oda, T. Kuriya, and M. Fujishima, Graphical Evaluation Method for Void Distribution in Direct Energy Deposition, *Procedia Manufacturing,* vol. 6, pp. 105-112, 2016.
[27] W. E. Frazier, Metal Additive Manufacturing: A Review, *Journal of Materials Engineering and Performance,* vol. 23, no. 6, pp. 1917-1928, 2014.
[28] M. Vaezi, H. Seitz, and S. Yang, A review on 3D micro-additive manufacturing technologies, *The International Journal of Advanced Manufacturing Technology,* vol. 67, no. 5-8, pp. 1721-1754, 2012.
[29] B. Herren, T. Gu, Q. Tang, M. Saha, and Y. Liu, 3D Printing and Stretching Effects on Alignment Microstructure in PDMS/CNT Nanocomposites, in *ASME International Mechanical Engineering Congress and Exposition*, 2019, vol. 59490, p. V012T10A019: American Society of Mechanical Engineers.
[30] M. Abshirini, M. Charara, M. C. Saha, M. C. Altan, and Y. Liu, Optimization of 3D Printed Elastomeric Nanocomposites for Flexible Strain Sensing Applications, in *ASME International Mechanical Engineering Congress and Exposition,* 2019, vol. 59360, p. V001T03A013: American Society of Mechanical Engineers.
[31] M. Abshirini, M. Charara, Y. Liu, M. Saha, and M. C. Altan, 3D printing of highly stretchable strain sensors based on carbon nanotube nanocomposites, *Advanced Engineering Materials,* vol. 20, no. 10, p. 1800425, 2018.

[32] M. Vaezi, H. Seitz, and S. Yang, A review on 3D micro-additive manufacturing technologies, *The International Journal of Advanced Manufacturing Technology,* vol. 67, no. 5-8, pp. 1721-1754, 2013.
[33] R. D. Farahani, K. Chizari, and D. Therriault, Three-dimensional printing of freeform helical microstructures: a review, *Nanoscale,* vol. 6, no. 18, pp. 10470-85, Sep 21 2014.
[34] Q. Mu, C. K. Dunn, L. Wang, M. L. Dunn, H. J. Qi, and T. Wang, Thermal cure effects on electromechanical properties of conductive wires by direct ink write for 4D printing and soft machines, *Smart Materials and Structures,* vol. 26, no. 4, 2017.
[35] A. Mondal, M. Sukati, M. Charara, M. C. Saha, Y. Liu, S. Patterson, and T. Robison, Investigation of Rheology and 3D Printability of PDMS Nanocomposites Ink, in *Proceedings of the American Society for Composites—Thirty-fourth Technical Conference*, 2019.
[36] J. Cesarano, A Review of Robocasting Technology, *MRS Proceedings,* vol. 542, 2011.
[37] J. T. Muth, D. M. Vogt, R. L. Truby, Y. Menguc, D. B. Kolesky, R. J. Wood, and J. A. Lewis, Embedded 3D printing of strain sensors within highly stretchable elastomers, *Adv Mater,* vol. 26, no. 36, pp. 6307-12, Sep 2014.
[38] B. Herren, M. Charara, M. C. Saha, M. C. Altan, and Y. Liu, Rapid Microwave Polymerization of Porous Nanocomposites with Piezoresistive Sensing Function, *Nanomaterials,* vol. 10, no. 2, p. 233, 2020.
[39] B. Herren, M. C. Saha, and Y. Liu, Carbon Nanotube-Based Piezoresistive Sensors Fabricated by Microwave Irradiation, *Advanced Engineering Materials,* p. 1901068, 2019.
[40] B. Herren, P. Larson, M. C. Saha, and Y. Liu, Enhanced Electrical Conductivity of Carbon Nanotube-Based Elastomer Nanocomposites Prepared by Microwave Curing, *Polymers,* vol. 11, no. 7, p. 1212, 2019.
[41] R. Matsuzaki, M. Ueda, M. Namiki, T. K. Jeong, H. Asahara, K. Horiguchi, T. Nakamura, A. Todoroki, and Y. Hirano, Three-dimensional printing of continuous-fiber composites by in-nozzle impregnation, *Sci Rep,* vol. 6, p. 23058, Mar 11 2016.
[42] X. Tian, T. Liu, C. Yang, Q. Wang, and D. Li, Interface and performance of 3D printed continuous carbon fiber reinforced PLA composites, *Composites Part A: Applied Science and Manufacturing,* vol. 88, pp. 198-205, 2016.
[43] Y. Ming, Y. Duan, B. Wang, H. Xiao, and X. Zhang, A Novel Route to Fabricate High-Performance 3D Printed Continuous Fiber-Reinforced Thermosetting Polymer Composites, *Materials (Basel),* vol. 12, no. 9, Apr 26 2019.
[44] C. Composites. (February 17). *Technology*. Available: https://www.continuouscomposites.com/technology
[45] C. Naramore. (2020, February 17). *Intro to Continuous Fiber 3D Printing*. Available: https://3dprinting.com/3d-printing-use-cases/continuous-fiber-3d-printing/
[46] O. Industries. (April 13). *The Difference Between Thermoplastic and Thermosetting Plastic*. Available: https://www.osborneindustries.com/news/difference-between-thermoplastic-thermosetting-plastic/
[47] Makerbot. (April 9). *Makerbot PLA*. Available: https://www.makerbot.com/3d-printers/materials/method-pla/
[48] Makerbot. (April 9). *Makerbot ABS*. Available: https://www.makerbot.com/3d-printers/materials/method-abs/
[49] C. P. Solutions. (April 9). *PR48 Technical Data Sheet*.

[50] L. Corporation. (2012, April 9). *Thermoset EP-20 Epoxy Resin*.
[51] H. L. Tekinalp, V. Kunc, G. M. Velez-Garcia, C. E. Duty, L. J. Love, A. K. Naskar, C. A. Blue, and S. Ozcan, Highly oriented carbon fiber–polymer composites via additive manufacturing, *Composites Science and Technology*, vol. 105, pp. 144-150, 2014.
[52] G. W. Melenka, B. K. O. Cheung, J. S. Schofield, M. R. Dawson, and J. P. Carey, Evaluation and prediction of the tensile properties of continuous fiber-reinforced 3D printed structures, *Composite Structures*, vol. 153, pp. 866-875, 2016.
[53] MatWeb. (April 9). *Hexcel HexTow AS4C 3K Standard Modulus Carbon Fiber* Available: http://www.matweb.com/search/DataSheet.aspx?MatGUID=b3edd4205cad4af68377c77faf9476be
[54] MatWeb. (April 9). *E-Glass Fiber, Generic*. Available: http://www.matweb.com/search/datasheet.aspx?matguid=d9c18047c49147a2a7c0b0bb1743e812
[55] MatWeb. (April 9). *DuPont Kevlar 49 Aramid Fiber*. Available: http://www.matweb.com/search/datasheet.aspx?matguid=77b5205f0dcc43bb8cbe6fee7d36cbb5
[56] Creality. (April 5). *Creality CR-10 Mini 3D Printer*. Available: https://www.creality3d.shop/collections/cr-series/products/creality3d-cr-10mini-3d-printer-with-resume-print-300x220x300mm
[57] GitHub. (April 5). *Shenzhen Creality 3D Technology Co.* Available: https://github.com/Creality3DPrinting
[58] A. Composites. (April 5). *Carbon Fiber Tow*. Available: https://store.acpsales.com/products/2107/carbon-fiber-tow
[59] D. Microfluidics. (April 5). *Needle gauge table*. Available: https://darwin-microfluidics.com/blogs/tools/syringe-needle-gauge-table
[60] Amazon. (April 5). *Luer Lock Blunt Needles Dispensing Syringe Needle Tips*. Available: https://www.amazon.com/Needles-Dispensing-Syringe-Needle-Pieces/dp/B07FSNQ7W1
[61] Autodesk. (April 5). *Autodesk Standard Clear Prototyping Resin (PR48)*.
[62] C. P. Solutions. (April 13). *DLP Prototyping Materials*. Available: https://www.cpspolymers.com/dlp
[63] Autodesk. (2015, April 5). *PR48 Material Safety Data Sheet*.
[64] C. Aulin, S. Ahola, P. Josefsson, T. Nishino, Y. Hirose, M. Österberg, and L. Wågberg, Nanoscale Cellulose Films with Different Crystallinities and Mesostructures・ Their Surface Properties and Interaction with Water, *Langmuir*, vol. 25, no. 13, pp. 7675-7685, 2009.
[65] X. Wu, R. J. Moon, and A. Martini, Crystalline cellulose elastic modulus predicted by atomistic models of uniform deformation and nanoscale indentation, *Cellulose*, vol. 20, no. 1, pp. 43-55, 2013.
[66] J. Wang, B. Weng, P. Larson, and Y. Liu, Synthesis and characterization of self-assembled ZnO nanoarrays on hybrid structural fibers, *Surfaces and Interfaces*, vol. 16, pp. 188-193, 2019.
[67] W. Luo, M. Charara, M. C. Saha, and Y. Liu, Fabrication and characterization of porous CNF/PDMS nanocomposites for sensing applications, *Applied Nanoscience*, vol. 9, no. 6, pp. 1309-1317, 2019.

[68] M. Charara, M. Abshirini, M. C. Saha, M. C. Altan, and Y. Liu, Highly sensitive compression sensors using three-dimensional printed polydimethylsiloxane/carbon nanotube nanocomposites, *Journal of Intelligent Material Systems and Structures,* vol. 30, no. 8, pp. 1216-1224, 2019.
[69] S. A. Chowdhury, M. C. Saha, S. Patterson, T. Robison, and Y. Liu, Highly conductive polydimethylsiloxane/carbon nanofiber composites for flexible sensor applications, *Advanced Materials Technologies,* vol. 4, no. 1, p. 1800398, 2019.
[70] J. Wang, B. Weng, P. Larson, and Y. Liu, Synthesis of ZnO nanoarrays on carbon fibers using combined atomic layer deposition and hydrothermal methods, *Materials Research Express,* vol. 5, no. 6, p. 065029, 2018.
[71] R. F. Gibson, A review of recent research on mechanics of multifunctional composite materials and structures, *Composite structures,* vol. 92, no. 12, pp. 2793-2810, 2010.
[72] J. Zhang, B. Koo, Y. Liu, J. Zou, A. Chattopadhyay, and L. Dai, A novel statistical spring-bead based network model for self-sensing smart polymer materials, *Smart Materials and Structures,* vol. 24, no. 8, p. 085022, 2015.
[73] Y. Liu, A. Rajadas, and A. Chattopadhyay, A biomimetic structural health monitoring approach using carbon nanotubes, *Jom,* vol. 64, no. 7, pp. 802-807, 2012.
[74] J. Zou, Y. Liu, A. Chattopadhyay, and L. Dai, A self-sensing fiber reinforced polymer composite using mechanophore-based smart polymer, in *Behavior and Mechanics of Multifunctional Materials and Composites 2015*, 2015, vol. 9432, p. 943204: International Society for Optics and Photonics.
[75] M. Charara, W. Luo, M. C. Saha, and Y. Liu, Investigation of lightweight and flexible carbon nanofiber/poly dimethylsiloxane nanocomposite sponge for piezoresistive sensor application, *Advanced Engineering Materials,* vol. 21, no. 5, p. 1801068, 2019.
[76] S. Wang, J. Echeverry, L. Trevisi, K. Prather, L. Xiang, and Y. Liu, Ultrahigh Resolution Pulsed Laser-Induced Photoacoustic Detection of Multi-Scale Damage in CFRP Composites, *Applied Sciences,* vol. 10, no. 6, p. 2106, 2020.
[77] S. Wang, T. Tran, L. Xiang, and Y. Liu, Non-Destructive Evaluation of Composite and Metallic Structures using Photo-Acoustic Method, in *AIAA Scitech 2019 Forum*, 2019, p. 2042.
[78] S. Wang, L. Xiang, Y. Liu, and H. Liu, Photo-Acoustic Based Non-Contact and Non-Destructive Evaluation for Detection of Damage Precursors in Composites, in *ASME 2018 International Mechanical Engineering Congress and Exposition*, 2018: American Society of Mechanical Engineers Digital Collection.
[79] J. P. Lynch and K. J. Loh, A summary review of wireless sensors and sensor networks for structural health monitoring, *Shock and Vibration Digest,* vol. 38, no. 2, pp. 91-130, 2006.
[80] J. Ou and H. Li, Structural health monitoring in mainland China: review and future trends, *Structural health monitoring,* vol. 9, no. 3, pp. 219-231, 2010.
[81] Y. Liu and A. Chattopadhyay, Low-velocity impact damage monitoring of a sandwich composite wing, *Journal of Intelligent Material Systems and Structures,* vol. 24, no. 17, pp. 2074-2083, 2013.
[82] Y. Liu, J. Johnston, and A. Chattopadhyay, Non-Destructive evaluation of composite adhesive kissing bond, in *ASME 2013 International Mechanical Engineering Congress and Exposition*, 2013: American Society of Mechanical Engineers Digital Collection.

[83] Y. Liu and S. Nayak, Structural health monitoring: State of the art and perspectives, *Jom*, vol. 64, no. 7, pp. 789-792, 2012.
[84] T. Stepinski, T. Uhl, and W. Staszewski, *Advanced structural damage detection: from theory to engineering applications*. John Wiley & Sons, 2013.
[85] F.-G. Yuan, *Structural health monitoring (SHM) in aerospace structures*. Woodhead Publishing, 2016.
[86] Y. Liu, M. Y. Fard, A. Chattopadhyay, and D. Doyle, Damage assessment of CFRP composites using a time–frequency approach, *Journal of Intelligent Material Systems and Structures*, vol. 23, no. 4, pp. 397-413, 2012.
[87] Y. Liu, M. Yekani Fard, and A. Chattopadhyay, A Statistical Approach to Investigate Temperature Effects on Guided Wave Based Structural Health Monitoring, in *53rd AIAA/ASME/ASCE/AHS/ASC Structures, Structural Dynamics and Materials Conference 20th AIAA/ASME/AHS Adaptive Structures Conference 14th AIAA*, p. 1787.
[88] Y. Liu, S. B. Kim, A. Chattopadhyay, and D. Doyle, Application of system-identification techniquest to health monitoring of on-orbit satellite boom structures, *Journal of Spacecraft and Rockets*, vol. 48, no. 4, pp. 589-598, 2011.
[89] Y. Liu, M. Y. Fard, S. B. Kim, A. Chattopadhyay, and D. Doyle, Damage detection in composite structures using Lamb wave analysis and time-frequency approach, in *Sensors and Smart Structures Technologies for Civil, Mechanical, and Aerospace Systems 2011*, 2011, vol. 7981, p. 79813N: International Society for Optics and Photonics.
[90] V. Janapati, F. Kopsaftopoulos, F. Li, S. J. Lee, and F.-K. Chang, Damage detection sensitivity characterization of acousto-ultrasound-based structural health monitoring techniques, *Structural Health Monitoring*, vol. 15, no. 2, pp. 143-161, 2016.
[91] G. Alleman, M. Pelt, and R. Groves, Air-coupled ultrasound for damage detection in CFRP using Lamb waves and ultrasonic verification, in *Proc. ICAST2014: 25nd International Conference on Adaptive Structures and Technologies, The Hague*, 2014.
[92] L. Cot, C. Gómez, F. Gamboa, F. Kopsaftopoulos, and F. Chang, SHM-based fatigue damage prognostics in composite structures, in *8th European Workshop On Structural Health Monitoring (EWSHM 2016)*, 2016.
[93] Y. Liu, S. Mohanty, and A. Chattopadhyay, Condition based structural health monitoring and prognosis of composite structures under uniaxial and biaxial loading, *Journal of Nondestructive Evaluation*, vol. 29, no. 3, pp. 181-188, 2010.
[94] Y. Liu, S. Mohanty, and A. Chattopadhyay, A Gaussian process based prognostics framework for composite structures, in *Modeling, Signal Processing, and Control for Smart Structures 2009*, 2009, vol. 7286, p. 72860J: International Society for Optics and Photonics.
[95] S. S. Kessler, E. B. Flynn, C. T. Dunn, and M. D. Todd, A structural health monitoring software tool for optimization, diagnostics and prognostics, CALIFORNIA UNIV SAN DIEGO LA JOLLA2011.
[96] F.-K. Chang, *Structural Health Monitoring 2003: From Diagnostics & Prognostics to Structural Health Management: Proceedings of the 4th International Workshop on Structural Health Monitoring, Stanford University, Stanford, CA, September 15-17, 2003*. DEStech Publications, Inc, 2003.